



HAL
open science

IDENTIFICATION OF FIRST-IN-CLASS INHIBITORS OF KALLIKREIN-RELATED PEPTIDASE 6 THAT PROMOTE OLIGODENDROCYTE DIFFERENTIATION

Sabrina Aït Amiri, Cyrille Deboux, Feryel Soualmia, Nancy Chaaya, Maxime Louet, Eric Duplus, Sandrine Betuing, Brahim Nait Oumesmar, Nicolas Masurier, Chahrazade El Amri

► **To cite this version:**

Sabrina Aït Amiri, Cyrille Deboux, Feryel Soualmia, Nancy Chaaya, Maxime Louet, et al.. IDENTIFICATION OF FIRST-IN-CLASS INHIBITORS OF KALLIKREIN-RELATED PEPTIDASE 6 THAT PROMOTE OLIGODENDROCYTE DIFFERENTIATION. *Journal of Medicinal Chemistry*, 2021, 64 (9), pp. 5667-5688. 10.1021/acs.jmedchem.0c02175 . hal-03281511

HAL Id: hal-03281511

<https://hal.sorbonne-universite.fr/hal-03281511v1>

Submitted on 8 Jul 2021

HAL is a multi-disciplinary open access archive for the deposit and dissemination of scientific research documents, whether they are published or not. The documents may come from teaching and research institutions in France or abroad, or from public or private research centers.

L'archive ouverte pluridisciplinaire **HAL**, est destinée au dépôt et à la diffusion de documents scientifiques de niveau recherche, publiés ou non, émanant des établissements d'enseignement et de recherche français ou étrangers, des laboratoires publics ou privés.

IDENTIFICATION OF FIRST-IN-CLASS INHIBITORS OF KALLIKREIN-RELATED PEPTIDASE 6 THAT PROMOTE OLIGODENDROCYTE DIFFERENTIATION

Sabrina AÏT AMIRI¹ Cyrille DEBOUX², Feryel SOUALMIA¹, Nancy CHAAYA¹, Maxime LOUET³, Eric DUPLUS¹, Sandrine BETUING⁴, Brahim NAIT OUMESMAR^{2*}, Nicolas MASURIER^{3*}, Chahrazade EL AMRI^{1*}

1. Sorbonne Université, Faculty of Sciences and Engineering, IBPS, UMR 8256 CNRS-UPMC, ERL INSERM U1164, Biological Adaptation and Ageing, F-75252 Paris, France. Paris, France
2. Sorbonne Université, Inserm U 1127, CNRS UMR 7725, Institut du Cerveau, F-75013, Paris, France
3. Institut des Biomolécules Max Mousseron, Univ Montpellier, CNRS, ENSCM, Montpellier, France
4. Sorbonne Université, Faculty of Sciences and Engineering, IBPS, UMR 8246-CNRS / INSERM U1130 Neurosciences Paris Seine, F-75252 Paris, France. Paris, France

(*) Correspondence to C. El Amri (chahrazade.el_amri@sorbonne-universite.fr), B. Nait Oumesmar (brahim.nait_oumesmar@sorbonne-universite.fr); N. Masurier (nicolas.masurier@umontpellier.fr)

Abstract

Multiple sclerosis (MS) is an autoimmune demyelinating disease of the central nervous system (CNS) that causes severe motor, sensory and cognitive impairments. KLK6 is the most abundant serine protease secreted in the CNS, mainly by oligodendrocytes, the myelin-producing cells of the CNS, and KLK6 is assumed to be a robust biomarker of MS, since it is highly increased in the cerebrospinal fluid (CSF) of MS patients. Here, we report the design and biological evaluation of KLK6's low-molecular weight inhibitors, *para*-aminobenzyl derivatives. Interestingly, selected hit compounds were selective of KLK6 proteolytic network encompassing KLK1 and plasmin that also participate to the development of MS physiopathology. Moreover, hits were found non-cytotoxic on primary cultures of murine neurons and oligodendrocyte precursors (OPCs). Among them, two compounds (**32** and **42**) were shown to promote the differentiation of OPCs into mature oligodendrocytes *in vitro* constituting thus emerging leads for the development of regenerative therapies.

Keywords: Kallikrein-related peptidase 6; synthetic inhibitors; mechanism of inhibition; polypharmacology; demyelinating diseases; oligodendrocytes' maturation.

Introduction

Multiple sclerosis (MS) is a chronic inflammatory demyelinating disease of the central nervous system (CNS). MS affects more than two million people worldwide. ¹ In young adults, MS is the most common neurological disorder and the leading cause of severe non-traumatic disability. The main target of MS is the myelin sheath surrounding CNS axons in the brain, spinal cord and optic nerve. ¹ The myelin sheath is synthesized by oligodendrocytes that play a crucial role in the maintenance and functioning of neuronal networks. MS is associated with an inflammatory reaction of the CNS that results in degradation of the myelin sheath, therefore leading to diffuse demyelinating lesions. The consequences of this demyelination are multiple, nerve conduction is impaired and neurodegeneration occurs with disease progression. ² Moreover, myelin debris exacerbates the activation of immune pathways triggering demyelination. ³ Clinically, these disturbances result in severe motor, sensory and cognitive deficits. The lack of a regenerative therapy that prevents disease progression represents the greatest unmet medical in MS. Disease-modifying drugs in the market are mainly targeting the inflammatory components of the pathology, but have little impact on oligodendrocyte regeneration and remyelination. ⁴⁻⁶ The identification of new therapeutic compounds for MS-enhancing myelin repair is thus a critical public health issue. ^{7,8} A special effort may be put on the search for pharmacological compounds, capable of simultaneously modulating neuroinflammation and promoting myelin regeneration for a more complete health care of MS patients. There is thus an urgent need to identify and validate novel targets to reach this issue.

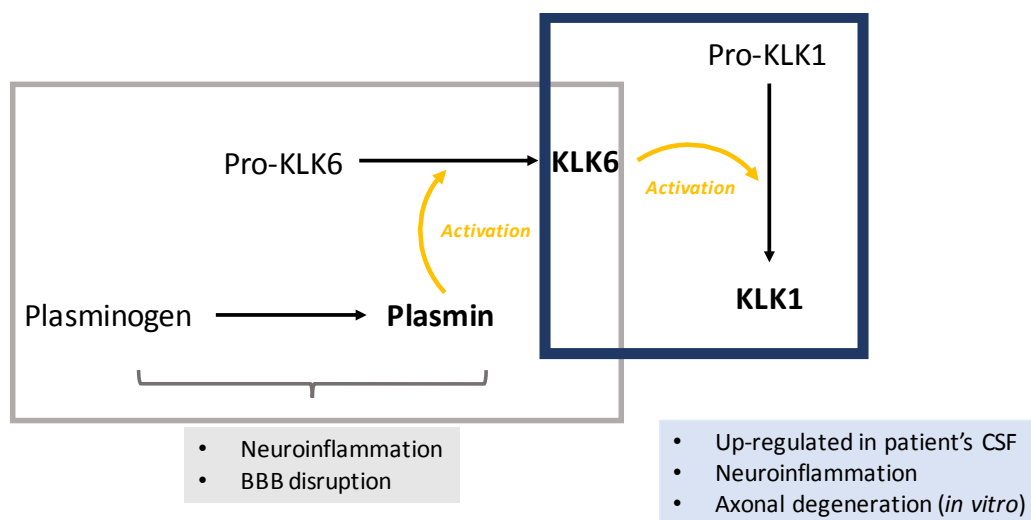
In adults, under normal physiological conditions, kallikrein-related peptidase 6 (KLK6) is strongly expressed by oligodendrocytes and can be detected in neurons, whereas it is very weakly expressed in astrocytes and resting microglia. ⁹ However, in response to a CNS lesion

1
2
3 such as glutamate-induced excitotoxicity, inflammation or traumatic injury, the level of KLK6
4
5 expression rises in oligodendrocytes and neurons, and its expression is induced in reactive
6
7 astrocytes and microglia. ¹⁰ Among the 15 tissue kallikreins, KLK6 is the most abundant in the
8
9 CNS, and is arguably the most abundant serine proteases produced in the CNS. ¹¹
10
11

12
13 KLK6 has a versatile action within the CNS. ⁹ Interestingly, KLK6 cleaves myelin proteins,
14
15 such as the myelin basic protein (MBP). KLK6 is a major protease of the process of
16
17 demyelination/remyelination of axons. ^{9,10,12} In addition to cleaving myelin proteins, KLK6 can
18
19 also degrade blood-brain barrier components such as laminin, fibronectin and collagen, and
20
21 induces inflammation *via* Protease Activated Receptors (PAR) activation and underlying
22
23 intracellular Ca²⁺ mobilization. It should also be noted that the use of recombinant KLK6 *in*
24
25 *vitro* contributes to neuronal lesions and oligodendroglipathies. ¹³ Some proteases have also
26
27 been suggested for the activation of KLK6 *in vivo*, including plasmin, a serine protease involved
28
29 in fibrinolysis. Finally, KLK6 is involved in oligodendrocyte differentiation and myelination
30
31 processes. Different studies support that KLK6 is involved in the pathophysiology of MS. ¹²⁻¹⁷
32
33 Firstly, patients with MS have abnormally high KLK6 levels in serum, cerebrospinal fluid (CSF)
34
35 and demyelinating lesions, which demonstrate the implication of this protease at different
36
37 levels of the pathology. ¹⁸ Secondly, KLK6 induces demyelination, both through excessive
38
39 cleavage of myelin proteins and deleterious effects on oligodendrocyte-process outgrowth
40
41 and differentiation, thus leading to a drastic reduction in the number of myelinating
42
43 oligodendrocytes. ¹⁹ Third, KLK6 participates in the neuroinflammatory process through the
44
45 overactivation of PAR receptors but also by increasing the expression of pro-inflammatory
46
47 cytokines. Therefore, KLK6 participates in the establishment of a toxic environment that leads
48
49 to demyelination and neurodegeneration, the main cause of disability progression in MS
50
51 patients. ¹⁹ KLK6 and KLK1 may also serve as serological markers of MS and may contribute
52
53
54
55
56
57
58
59
60

1
2
3 directly to neurodegeneration. Furthermore, the immunization of mice with recombinant
4
5 KLK6 antibodies significantly delayed onset and severity of clinical deficits in an experimental
6
7 autoimmune encephalomyelitis (EAE) mouse model of MS.^{12, 20} It is also well established that
8
9 the potential significance of proteolytic activity in MS not only relates to their use as potential
10
11 biomarkers but also as prospective therapeutic targets. The range of potential involvement of
12
13 proteolytic activity in MS pathogenesis extends from parenchymal degenerative events
14
15 including myelin destruction and axon injury, to release of antigenic self-epitopes, immune
16
17 cell activation, and permeabilization of the blood-brain barrier. Scarisbrick and co-workers
18
19 have proposed the term of MS degradome to encompass the set of proteases, substrates, and
20
21 endogenous protease inhibitors involved in development and progression of MS.¹⁹
22
23
24
25
26
27
28
29

30 **Scheme 1** summarizes the central role of KLK6 and its crosstalk with thrombolytic proteolytic
31
32 pathways, thus illustrating the early concept of MS degradome.²¹ Particularly, it has been
33
34 recently shown that plasminogen and plasmin-mediated fibrinolysis are key modifiers of the
35
36 onset of neuroinflammatory demyelination.^{22, 23} KLK1 was early shown to be a potential
37
38 serological marker of progressive MS and contribute directly to the development of
39
40 neurological disability by promoting axonal injury and neuron apoptosis.¹⁹
41
42
43
44
45
46
47
48
49
50
51
52
53
54
55
56
57
58
59
60



23 **Scheme 1:** Putative KLK6's pathological proteolytic network

24
25
26
27
28 In this context, the development of innovative inhibitors of KLK6 activity and its associated
29 proteolytic network appears as a new therapeutic avenue.

30
31
32
33
34
35 The aim of this study is thus to identify potent KLK6 inhibitors encompassing the
36 following properties: (i) reversibility, indeed non-covalent inhibitors, which are devoid of a
37 warhead, such as lack of specificity, instability and excessive reactivity. Considering the
38 physiological implication of KLK6 in the CNS homeostasis reversible inhibition would be
39 safer, and (ii) able to inhibit other proteases involved in the KLK6 proteolysis network, *i.e.*
40 KLK1 and plasmin. Herein, we identified and optimized original organic inhibitors for
41 KLK6 and its proteolytic network. The designed low molecular weight inhibitors are potent
42 and reversible towards KLK6, their inhibitory potency was also evaluated on a large panel of
43 proteases. We also provided a detailed structure-activity relationship and dissected out the
44 chemical basis for optimal inhibition. Hit compounds were found devoid of cytotoxic
45 effects towards
46
47
48
49
50
51
52
53
54
55
56
57
58
59
60

primary cultures of mouse neurons and oligodendrocyte precursors (OPCs), and displayed favorable drug-like characteristics. Interestingly, some hit compounds promoted OPC differentiation *in vitro*. These selected compounds constitute promising leads for the development of innovative myelination therapy.

Results and Discussion

Rational design of para-benzylamine derivatives

While the field of KLK's inhibitor discovery is relatively underdeveloped despite very huge interest in several therapeutic areas, recent reviews highlight the interest and need for further works.²⁴⁻²⁸

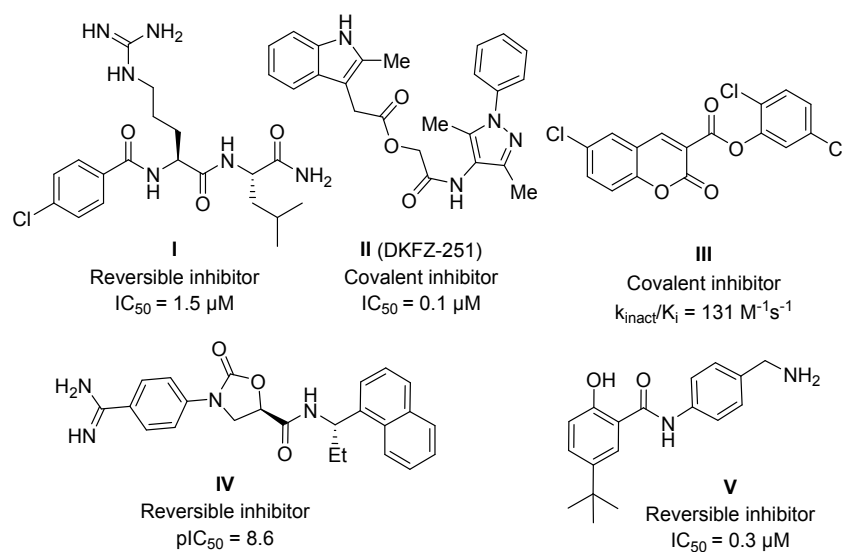


Chart 1: Main KLK6 inhibitors reported in the literature

A common approach for the development of inhibitors has been to use natural peptide inhibitors as starting points, exploiting combinatorial or designed mutations in order to achieve selectivity toward the targeted KLK (*e.g.* compound I, Chart 1).^{24, 28} However, the development of subtype selective KLK inhibitors remains challenging. Papo and collaborators

1
2
3 developed a yeast-displayed mutant library of the human amyloid precursor protein Kunitz
4 protease inhibitor domain (APPI) to derive serine protease inhibitors especially of KLK6.²⁹
5
6 Recently, Miller and co-workers have reported depsipeptides as potent KLK6's inhibitors to
7
8 derive activity-based probes (Compound II, Chart 1).³⁰ Our team has also recently identified
9
10 6-substituted coumarin-3-carboxylate derivatives as mechanism-based inhibitors (suicide
11
12 substrates, compound III, Chart 1).³¹ Several small molecules were also reported as reversible
13
14 inhibitors of KLK6. Among them, benzamidine and benzylamine derivatives are probably the
15
16 most potent inhibitors (*e.g.* compounds IV and V, Chart 1).^{32,33} Especially, *N*-(4-aminomethyl-
17
18 phenyl)-2-hydroxy-benzamide derivatives reported by Liang and co-workers are easily
19
20 accessible and can be subjected to a large chemical diversification for structure-activity
21
22 relationship (SAR) studies. Moreover, these compounds can potentially provide access to
23
24 submicromolar inhibitors. In this study, nine analogs were described and the 5-*tert*-butyl
25
26 derivative (compound V, Chart 1) revealed to be the most potent inhibitor of this series (IC_{50}
27
28 = 0.3 μ M) constituting an initial hit.³³ Substitution of the methylene group of the benzylamine
29
30 as well as alkylation at the amino nitrogen led to inactive compounds, which clearly
31
32 demonstrates that the amino group of the benzylamine is mandatory for the KLK6 inhibition.
33
34 X-ray structure obtained with one of the derivatives of this series revealed that the
35
36 benzylamine group bound into the S1 pocket of KLK6 by sharing a primary amine H-bonding
37
38 with the side chain of N189. The side chain of I218 is also an important factor to the binding
39
40 affinity through hydrophobic interaction with the phenyl ring of the benzylamine moiety. The
41
42 hydroxyl group of the phenol occupied the center of the oxyanion hole, forming an H-bonding
43
44 network with the backbone NH groups of G193 and S195 (**Figures 1A and B**). Keeping constant
45
46 these key elements involved in KLK6 interaction (**Figure 1C**), we synthesized and evaluated
47
48 novel series of *N*-(4-aminomethyl-phenyl)-2-hydroxy-benzamide and hydroxynaphtamide
49
50
51
52
53
54
55
56
57
58
59
60

derivatives and identified drug-like reversible organic inhibitors of KLK6 and its associated proteolytic network.

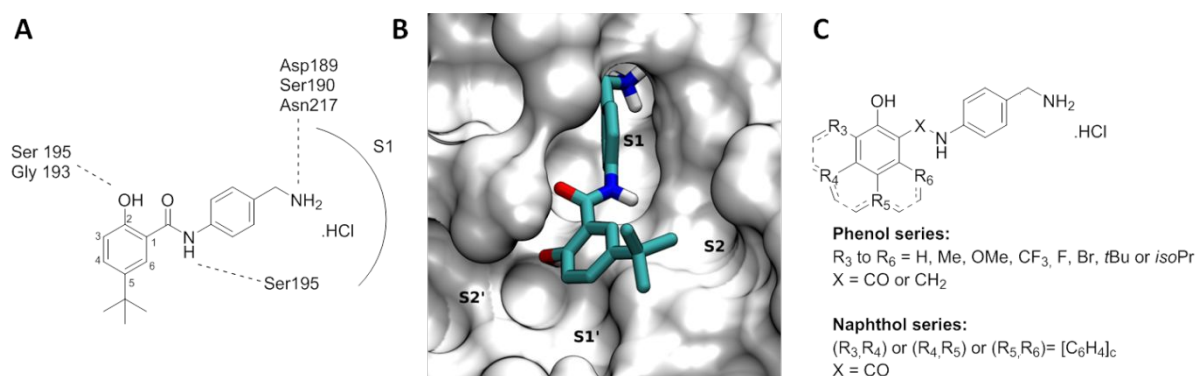
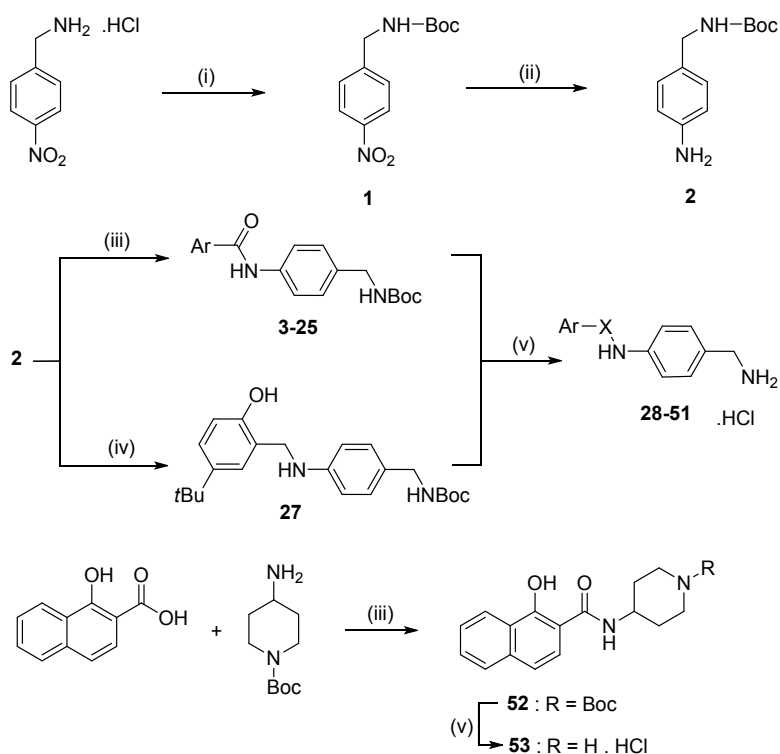


Figure 1: Rational design of *para*-amidobenzyl derivatives. **A.** Key interactions of compound **V** in the active site of KLK6 (H bonds are shown as dashed lines); **B.** Positioning of compound **V** in the S1 and S1' pockets of KLK6; **C.** Structures of studied compounds.

Targeted compounds, as well as the reference compound **V** (now named compound **28**) were synthesized as reported in Scheme 2.

Briefly, compound **2** was obtained in two steps from 4-nitrobenzylamine hydrochloride after Boc protection of the amine group, followed by the reduction of the nitro function. Compound **2** was then coupled with the appropriate salicylic or naphthoic acid in presence of EDCI (*N*-(3-dimethylaminopropyl)-*N*'-ethylcarbodiimide hydrochloride) to offer compounds **3-25** in moderate yields. Compound **27** was synthesized by reductive amination with aldehyde **26** in presence of sodium borohydride. Reaction between 1-naphthoic acid, 1-Boc-4-aminopiperidine and EDCI offered compound **52** in 64% yields. Finally, Boc group was removed using a mixture of hydrochloric acid in 1,4-dioxane to offer compounds **28-51** and **53** as hydrochloride salts.



Reagents and conditions: (i) Boc_2O , TEA, DCM, RT, 2h, 80%; (ii) H_2 , 10% Pd/C, AcOEt, RT, 4h, qt; (iii) ArCO_2H , EDCI, THF, reflux, 12h, 12-82%; (iv) 1. Compound **26**, EtOH, reflux, 6h; 2. NaBH_4 , RT, 1.5 h, 64% and (v) 6N HCl gaz in 1,4-dioxane, RT, 1.5 h, 44-99%.

Scheme 2: Synthesis of compounds **1** to **53**

Inhibitory potency hit compounds on KLK6 and on its proteolytic network

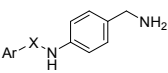
Newly synthesized compounds **28-51** and **53** were first screened on KLK6 through the evaluation of the percentage inhibition at 10 μM . This allows highlighting the promising compounds for the inhibition of KLK6. Among the 25 designed compounds, we preselected those raising an inhibition of at least 50% of the activity of KLK6 at a concentration of 10 μM and then determined their inhibitory potency through the quantification of IC_{50} .

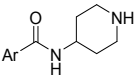
1
2
3 Starting from reference compound **28** (Table 1) previously identified by Liang and al. (2012a),
4
5 several modifications were studied in the phenol series, in order to determine key structural
6
7 elements for KLK6 inhibition. Suppression of the carbonyl group (compound **29**) as well as the
8
9 *tert*-butyl group (compound **30**) led to the loss of the activity. Then, sensitivity to the position
10
11 of the substituent carried out by the phenol group was observed in the methyl series
12
13 (compounds **31** to **34**). Substitution of position 4 and position 5, in a less extent, were the
14
15 most favorable to observe an optimal inhibition of KLK6. Several other groups were then
16
17 introduced into C4 and C5. These positions must be substituted by an apolar or bulky group
18
19 such as an isopropyl (compound **37**) or a methyl group (compound **32**) for C4 substituted
20
21 derivatives and a *tert*-butyl group (compound **28**) for C5 substituted derivatives. Interestingly,
22
23 the substitution of the C5 position by a halogen (compound **35**) or by a methoxy group
24
25 (compound **36**) is strongly unfavorable for the inhibition of KLK6.
26
27
28
29
30
31

32
33 When the inhibitor contains a naphthol group, a slight sensitivity with respect to the
34
35 position of the hydroxyl group is observed. Indeed, it must be substituted at positions 1 or 3
36
37 for optimal inhibition of KLK6 (compounds **40** and **42** respectively). More generally, the
38
39 hydroxyl group is essential because the inhibition of KLK6 decreases drastically when the
40
41 inhibitor contains a naphthyl (compound **43**) instead of a naphthol. This result is not surprising
42
43 because, in the phenol series, the hydroxyl group was reported to be involved into key
44
45 interactions notably with the S195 residue of KLK6. There is also a lack of inhibitory effect
46
47 when the compound contains an indolyl (compound **44**) or an oxoquinolyl ring (compound **45**)
48
49 in place of the naphthol ring, indicating that the hydroxyl group could not be replaced by
50
51 another hydrogen donor or acceptor (NH or ketone). Moreover, we noted the importance of
52
53 the benzylamine group. Indeed, we observed a significant decrease in the inhibition when this
54
55 same position is occupied by a piperidinyl group (compound **53**). Finally, several substitutions
56
57
58
59
60

into the naphthol ring were studied (compounds **47** to **51**, see supplementary information). However, all studied modifications led to autofluorescent compounds that could not be evaluated, except when a methoxy group was introduced on position 6 (compound **47**). In this case, a slight loss of activity compared to its unsubstituted analog (compound **40**) was observed.

Thus, among the new synthesized compounds, 5 new hits were identified in the series of *para*-aminobenzyl compounds (molecules **32**, **37**, **40**, **42** and **47**) (Table 1), displaying IC₅₀ equal or below 5 μM. The IC₅₀ accounts for the effectiveness of the inhibitor with respect to the enzyme and allows a prioritization according to the inhibitory power. The IC₅₀ values place compounds **32** and **42** at the top, while reference compound **28** (IC₅₀ = 9.06 μM) has one of the lowest efficacy with respect to KLK6 among the selected inhibitors.

Compound	Ar	X	% Inhibition at 10 μM or IC ₅₀ (μM)
			
28	5- <i>tert</i> -butyl-2-hydroxyphenyl	CO	9.06 ± 0.65
29	5- <i>tert</i> -butyl-2-hydroxyphenyl	CH ₂	NI
30	2-hydroxyphenyl	CO	14.83 %
31	3-methyl-2-hydroxyphenyl	CO	20%
32	4-methyl-2-hydroxyphenyl	CO	2.37 ± 0.12
33	5-methyl-2-hydroxyphenyl	CO	26.47 %
34	6-methyl-2-hydroxyphenyl	CO	7.27 %
35	5-bromo-2-hydroxyphenyl	CO	29.98 %
36	5-methoxy-2-hydroxyphenyl	CO	21.83 %
37	4-isopropyl-2-hydroxyphenyl	CO	3.63 ± 0.1
38	4-trifluoromethyl-2-hydroxyphenyl	CO	47 %

39	4-fluoro-2-hydroxyphenyl	CO	NI
40	1-hydroxy-2-naphthyl	CO	6.90 ± 0.24
41	2-hydroxy-1-naphthyl	CO	NI
42	3-hydroxy-2-naphthyl	CO	1.57 ± 0.03
43	2-naphthyl	CO	19.81 %
44	1-indolyl	CO	NI
45	4-oxo-3-quinolyl	CO	NI
46	2-pyridin-3-ol	CO	8.86%
47	6-methoxy-1-hydroxy-2-naphthyl	CO	7.18 ± 0.33
Compound	Ar	% Inhibition at 10 μM	
			
53	1-hydroxy-2-naphthyl		NI

1
2
3
4
5
6
7
8
9
10
11
12
13
14
15
16
17
18
19
20
21
22
23
24
25
26
27
28
29
30
31
32
33
34
35
36
37
38
39
40
41
42
43
44
45
46
47
48
49
50
51
52
53
54
55
56
57
58
59
60

1
2
3 **Table 1: Efficacy of *para*-aminobenzyl compounds towards KLK6.** For each compound, the inhibitory effect was quantified either by the percentage inhibition of KLK6 at 10 μ M, or by the IC_{50} for compound hits. To determine the IC_{50} , compounds at different concentrations (concentration ranges adjusted depending of the inhibitory potency) are pre-incubated 15 minutes at 37°C with KLK6 (2 nM). The enzymatic reaction is triggered by the addition of the Boc-QAR-AMC substrate (100 μ M) in 50mM Tris buffer, 1M Citrate 0.05% Brij-35; pH 7.4 at 37 °C. NA: not applicable. NI: non-inhibitor. The data result from at least three independent experiments in duplicate. The IC_{50} values were calculated by fitting the experimental data to eq. 2a or eq.2b and expressed as geometric standard deviation.

14 Then, we assessed inhibitory potency of our hit compounds (**32**, **37**, **40**, **42** and **47**) and of
15 reference compound **28** towards KLK1 and plasmin, as these two proteases are thought to be
16 part of the proteolytic network of KLK6 in MS.¹⁹ All these *para*-aminobenzyl derivatives lead
17 to at least 50% inhibition of the plasmin activity except inhibitor **28** (45%) while all the tested
18 inhibitors lead to an inhibition of at least 50% of KLK1 activity at a concentration of 10 μ M
19 (data not shown). The inhibitory potency (IC_{50}) of hit compounds was then determined. The
20 IC_{50} values with respect to plasmin place compound **47** (IC_{50} =3.3 μ M) at the top while reference
21 compound **28** (IC_{50} =21.3 μ M) has one of the lowest efficiency (**Table 2**). At the same time,
22 compound **42** is characterized by and IC_{50} value of 5.1 μ M towards KLK1, while other
23 compounds showed lower inhibitory potency and were thus not selected for further
24 mechanistic studies (**Table 2**).

Compound	Ar	X	IC ₅₀ (μM)	
			Plasmin	KLK1
28	5- <i>tert</i> -butyl-2-hydroxyphenyl	CO	21.3 ± 3.6	38.6 ± 1.9
32	4-methyl-2-Hydroxyphenyl	CO	9.2 ± 0.6	26.3 ± 1.1
37	4-isopropyl-2-Hydroxyphenyl	CO	4.8 ± 0.2	8.4 ± 0.3
40	1-hydroxy-2-Naphthyl	CO	10.2 ± 0.6	21.3 ± 1.6
42	3-hydroxy-2-Naphthyl	CO	7.4 ± 0.6	5.1 ± 0.2
47	6-methoxy-1-hydroxy-2-naphthyl	CO	3.3 ± 0.2	16.1 ± 0.4
49	7-methyl-1-hydroxy-2-naphthyl	CO	6.7 ± 0.6	49.4 ± 4

Table 2: Efficacy of KLK6 *para*-amino benzyl hit inhibitors on Plasmin and KLK1. For each compound, the inhibitory effect was quantified by the IC₅₀. To determine the IC₅₀, compounds at different concentrations (from 100 to 1.56 μM) are pre-incubated 15 minutes at 37°C with Plasmin (3 nM) or KLK1 (0,75 nM) in 50mM Tris buffer, 1M Citrate 0.05% Brij-35; pH 7.4 at 37 °C. The enzymatic reaction is then triggered by the addition of the Boc-QAR-AMC substrate (100 μM) for Plasmin and H-PFR-AMC substrate (100 μM) for KLK1. The data result from at least three independent experiments in duplicate. The IC₅₀ values were calculated by fitting the experimental data to eq. 2a or eq.2b and expressed as geometric standard deviation.

Hit compounds (**32**, **37**, **40**, **42**, **47**, **49**) and reference compound **28** were assessed by the evaluation of their selectivity spectrum against a set serine proteases and proteases involved in CNS homeostasis. **Table 3** provides an overview of putative cross-inhibition within a large set of proteases both serine proteases challenging in the CNS (KLK8, tPA, thrombin, trypsin, trypsin 3, KLK11) but also other kallikreins (KLK3, KLK4, KLK5, KLK14), matriptase, and diverse

1
2
3 proteases involved in CNS inflammation (Caspase-2, Caspase-3, Caspase-6, Cathepsin L).
4
5 Overall, this screening shows that hit compounds **32** and **42** have little effect on these selected
6
7 challenging proteases in contrast to the other identified inhibitors (**28, 37, 40, 47, 49**) that
8
9 display significant inhibition on several proteases. This allows to conclude that compounds **32**
10
11 and **42** are quite specific to KLK6 and its proximal proteolytic network.
12
13
14
15
16
17

<i>Inhibitor</i>	28	32	37	40	42	47	49
<i>Protease</i>							
KLK4	0	0	45	14	2	3	6
KLK5	35	5	24	22	4	31	0
KLK7	9	12	7	0	6	10	11
KLK8*	16	34	58	22	61	45	53
KLK11*	56	39	75	80	45	0	88
KLK13	5	10	15	2	19	0	12
KLK14	1.5	3	12	11	5	16	4
Caspase-2*	5	0	15	30	4	14	8
Caspase-3	11	0	13	10	5	3	10
Caspase-6*	13	5	12	56	40	70	31
Cathepsin L*	20	32	1	30	25	28	27
Matriptase	0	0	13	29	8	37	0
Thrombin	2	0	32	5	0	6	6
tPA	11	0	6	18	6	10	9
Trypsin	5	15	91	34	25	41	32
Trypsin 3*	15	20	73	30	36	32	21

18
19
20
21
22
23
24
25
26
27
28
29
30
31
32
33
34
35
36
37
38
39
40
41
42
43
44
45
46
47
48
49
50
51
52
53
54
55
56
57
58
59
60

Table 3: Selectivity of the inhibition of hit compounds toward selected CNS concurrent proteases (Inhibition percentage at 10 μ M, %). Each inhibitor (10 μ M) is preincubated with the enzyme at the optimal concentration for 15 minutes at 37°C. The reaction is triggered by the addition of the specific AMC-substrate in the appropriate buffer (cf section “Material and Methods – Selectivity profiling”). The data result from at least three independent experiments with a standard deviation < 10%. * **Proteases implicated in the CNS physiological processes. Gray light: significative percentage of inhibition.**

Mechanism of inhibition: hit compounds

Mechanistic studies were only performed for hit compound that display an ideal balance between potency and selectivity profiles towards KLK6 and its proximal proteolytic network (KLK1 and Plasmin) as well as the reference compound **28** for comparison. The reversibility of the inhibitions exerted by the compounds on KLK6 and its proteolytic network (Plasmin and KLK1) were demonstrated by the dilution method as described in the "Materials and methods" section. This experiment distinguishes an irreversible covalent inhibitor from a reversible one. Whatever the compound tested, a 1/100 dilution of the enzyme-inhibitor complex allowed restoring the initial activity of KLK6 to more than 80%. Hence, hit compounds are reversible inhibitors (**Figure 2**). The mechanisms were determined using representations of Dixon for hits and reference compounds. The results are shown in **Figure 2**. The Dixon graphs obtained for compounds **28**, **32** and **40** (**Figures 2A**, **2B** and **2C**) are typical of competitive inhibitors. Compounds **28**, **32** and **40** have K_i values of 4.3 μM , 2 μM and 2.4 μM , respectively. Surprisingly the mechanistic profile of compound **42** was found compatible with a noncompetitive inhibition with a K_i value of 0.8 μM which may be indicative of a more complex binding (**Figures 2D**). The Dixon plots for compounds **37** and **47** are provided in the supplementary data section (**Figure S1**).

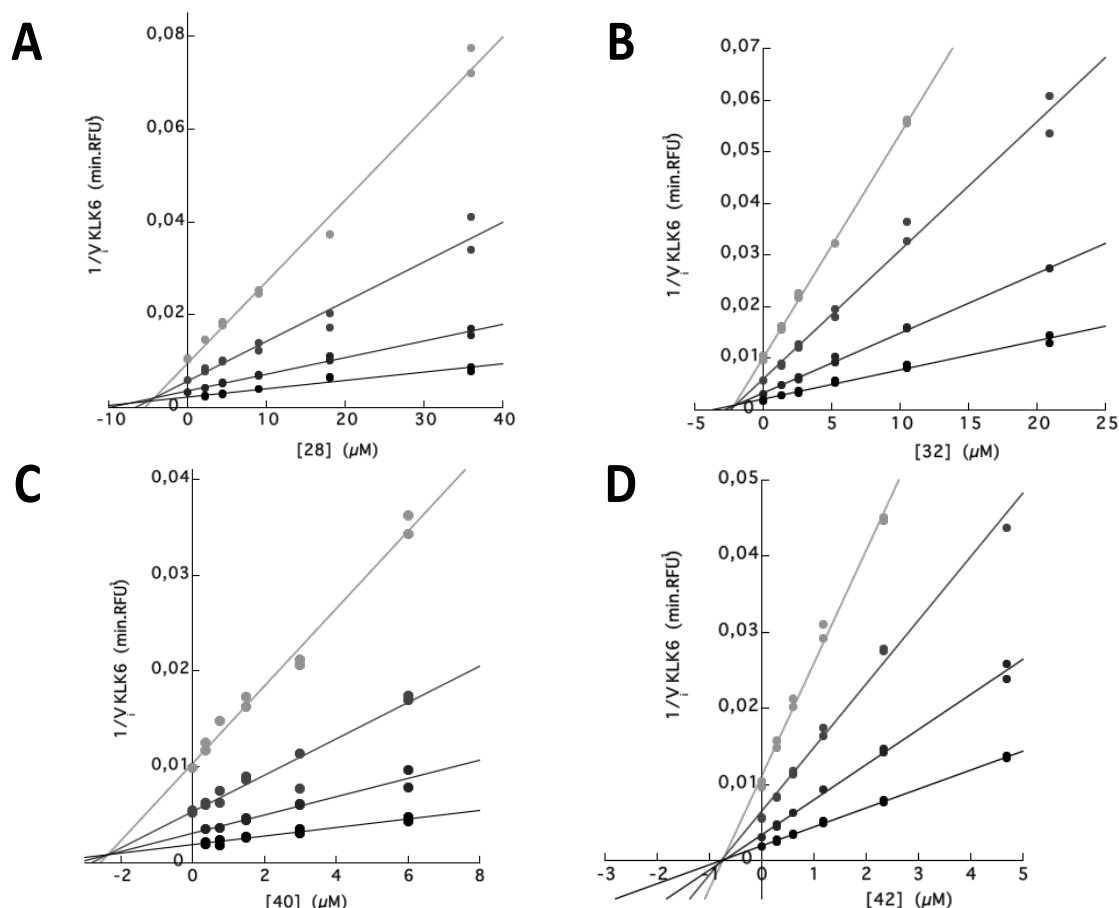


Figure 2: Mechanisms of inhibition towards KLK6. Dixon plots for inhibitors **28** (A), **32** (B), **40** (C) and **42** (D). Inhibitors at different concentrations (1/4; 1/2; 1; 2; 4 of the IC_{50} value) were tested using 2 nM KLK6 with substrate Boc-QAR-AMC at different concentrations (125; 62.5; 31.25; 15.625 μ M) in 50 mM Tris, 1 M Citrate, 0.05% Brij-35, pH 7 buffer at 37 °C.

Concerning plasmin and KLK1, all compounds are reversible inhibitors as shown using the dilution method. Dixon plots obtained for compounds **28**, **40** and **42** (Figures 3A, 3B and 3C) are typical of competitive inhibitors towards plasmin. Compounds **28**, **40** and **42** have K_i values of 14.5 μ M, 1.5 μ M and 1.3 μ M respectively. The Dixon plot for KLK1 obtained with inhibitor **42** is also typical of a competitive inhibitor ($K_i=2.4$ μ M) (Figure 3D and Table 4). Hence, it is shown that some of our hit KLK6 inhibitors also target key serine proteases of KLK6 proteolytic network with a relatively good affinity, which may constitute interesting perspective for a polypharmacological strategy.

Compound	<i>KLK6</i>		<i>Plasmin</i>		<i>KLK1</i>	
	Type of inhibition	K_i (μM)	Type of inhibition	K_i (μM)	Type of inhibition	K_i (μM)
28	Competitive	4.3 ± 1.6	Competitive	14.5 ± 1.2	NA	NA
32	Competitive	2 ± 0.5	NA	NA	NA	NA
37	Competitive	1.5 ± 0.2	NA	NA	NA	NA
40	Competitive	2.4 ± 0.1	Competitive	1.5 ± 0.5	NA	NA

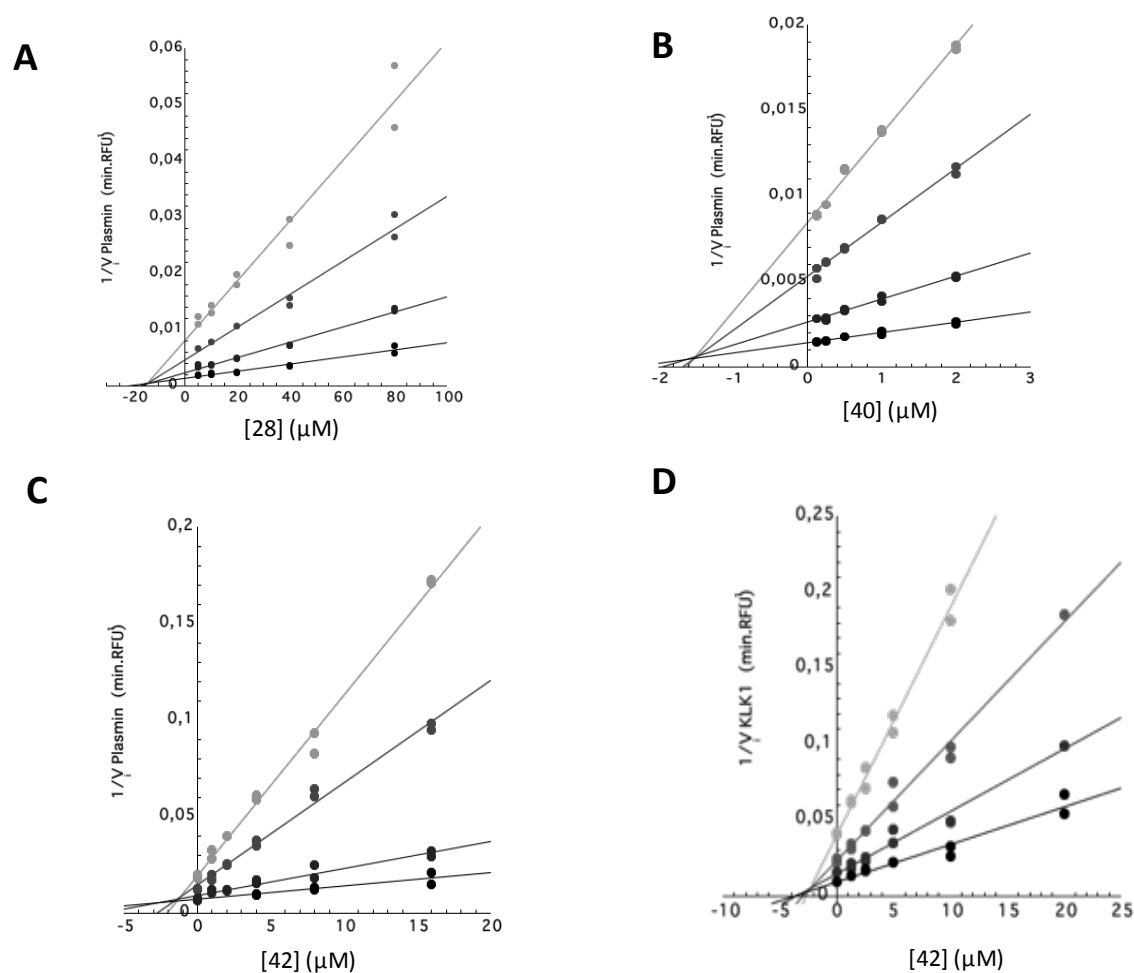


Figure 3: Mechanisms of inhibition towards KLK1 and plasmin. (A-C) Dixon plots for inhibitors **28** (A), **40** (B), **42** (C) towards plasmin. **(D)** Dixon plot for inhibitor **42** towards KLK1. Inhibitors at concentrations (1/4; 1/2; 1; 2; 4 of the IC_{50} value) were tested on plasmin (3 nM) or KLK1 (0,75 nM) with respectively Boc-QAR-AMC or H-PFR-AMC substrates at concentrations (125; 62.5; 31.25; 15.625 μM) in 50 mM Tris buffer, 1 M Citrate, 0.05% Brij-35, pH 7 at 37 °C.

42	Non-competitive	0.8 ± 0.3	Competitive	1.3 ± 0.53	Competitive	2.4 ± 0.5
47	Competitive	1 ± 0,3	NA	NA	NA	NA

Table 4: Mechanisms of inhibition and K_i values of hit compounds on KLK6 and its associated proteolytic network (KLK1 and plasmin). NA, not applicable

Evaluation of the cytotoxicity of hit compounds toward neural cells

To ensure that hit compounds (**32**, **40** and **42**) may constitute good starting points for further applications, their potential cytotoxicity toward neural cells was first evaluated in comparison to reference compound **28** on primary cultures of mouse cortical and striatal neurons at 10, 25, 50 and 100 μM (**Figure 4A**). Compounds **32** and **42** showed similar effects on both cortical and striatal neurons. A slight effect is observed from a concentration of 50 μM of inhibitors **32** and **42**, with percentages of cell survival around 65-70%. In contrast, compound **40** is the only compound showing a cytotoxic effect on striatal neurons from a concentration of 10 μM , this cytotoxicity is stable over the concentration range meaning that a plateau may be reached (**Figure 4B**). Thus, these newly identified inhibitors are all very poorly cytotoxic in comparison with the reference inhibitor **28**, which displays a noticeable cytotoxic effect, even at 25 μM , very close to the treatment with rotenone vehicle at 50 μM .

Hence, since compounds **32**, **40** and **42** did not show toxic effects towards neurons, they were selected for further studies in oligodendrocyte precursor cell (OPC) cultures as relevant biological model for MS.

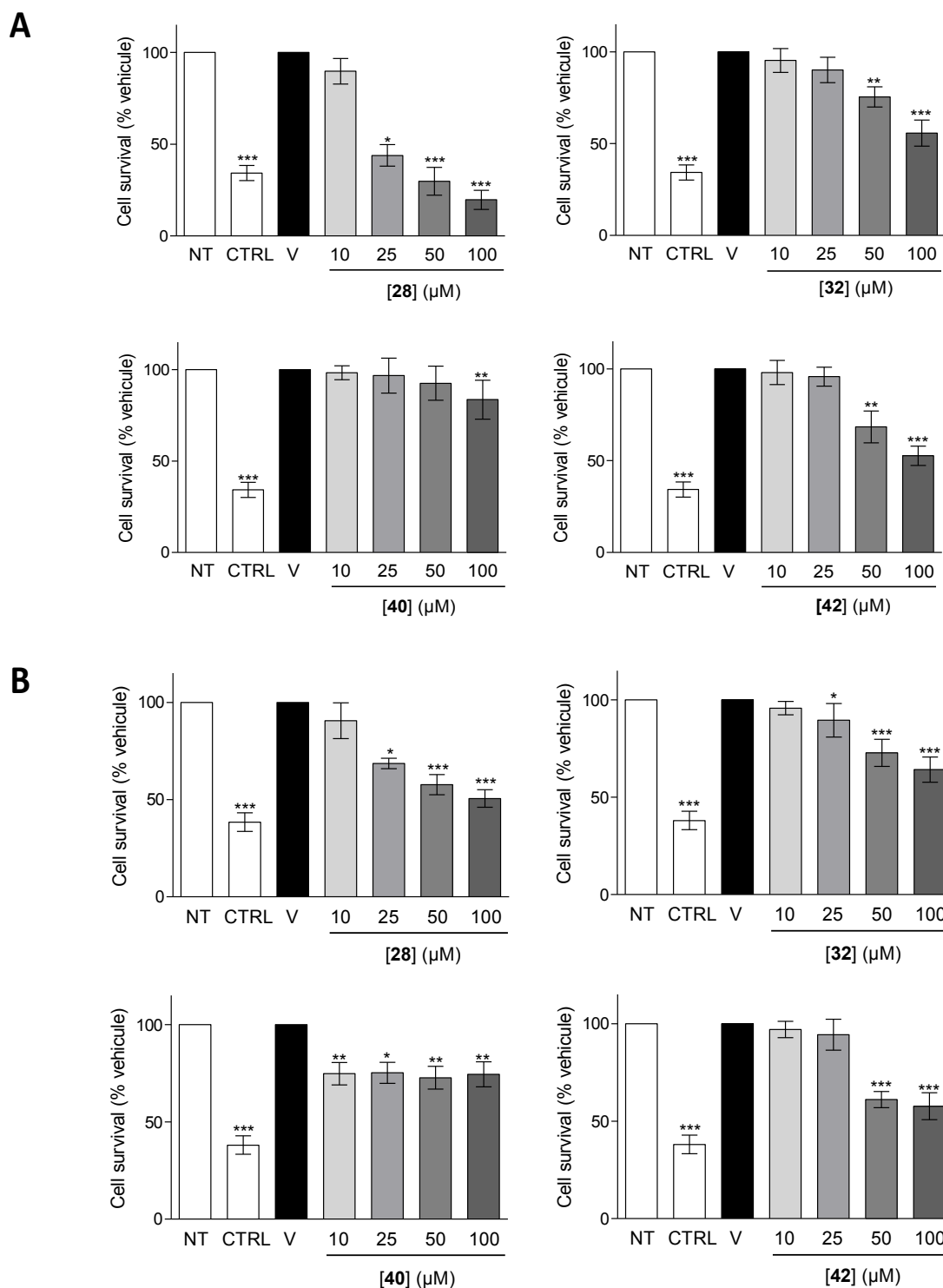


Figure 4: Cytotoxicity of hit inhibitors (32, 40 and 42) and reference compound 28 against primary cultures of cortical and striatal neurons. A – Cortical neurons. B- Striatal neurons. Primary cultures were treated either with inhibitors in a concentration range from 10 μM to 100 μM or with the vehicle (DMSO 1%, "V") or with rotenone 50 μM (CTRL) for 24 hours (N=3). Cell survival was then measured using XTT assay. All data sets were compared to the vehicle condition (V) for the generation of the p-values. * p-value < 0.05; ** p-value < 0.01; *** p-value < 0.001 (Kruskal-Wallis test). NT: no treatment

Pro-differentiating effect of hit compounds

Oligodendrocytes are derived from OPCs, a class of progenitors highly abundant during development but also persistent in the adult CNS, where they contribute to myelin remodelling and remyelination following acute demyelination. Although efficient remyelination occurs in the early stages of MS, it becomes inefficient and ultimately fails with disease progression. Remyelination requires the generation of new mature oligodendrocytes (OLs) from OPCs that must be recruited to the demyelinated lesions. Over the last decade, there have been huge interest in developing medicines to improve remyelination in MS.³⁴ The approaches range widely, from developing novel medicines and repurposing existing drugs. We thus assayed hit compounds on CG4 cell line and rat OPC primary cultures to check for their ability to induce differentiation. To monitor OPC differentiation, we developed a stable CG4 cell line expressing the GFP reporter at all stages of the oligodendroglial lineage cells and the mCherry reporter only in mature oligodendrocytes (**Figure 5A**). This innovative cellular assay allows the screening of promyelinating compounds based on the detection of fluorescence parameters. Indeed, both morphological changes and generation of mature oligodendrocytes can be monitored in a single assay, based on EGFP and mCherry fluorescence, respectively. After few days in basal medium, CG4 cells start to differentiate and expressed mCherry (**Figure 5B, 5C**). Fluorescence imaging (90 image fields were acquired for each condition) and quantification were performed with the Arrayscan XTI Imaging System. For each concentration tested, we quantified the number of mCherry⁺ cells and data were normalized relatively to control (N1 basal medium). 9cis retinoic acid (9cis-RA), a well-known compound promoting OPC differentiation was used a positive control.⁵³

Our data revealed no statistically significant change in the number of mCherry⁺ cells after treatments with compounds **40** (**Figure 5F**). For compound **28**, a significant increase of the

1
2
3 number of mCherry+ oligodendrocytes was observed at 2 μ M, while treatments at higher
4
5 concentrations ranging from 10 μ M to 30 μ M lead to a complete loss of cells (**Figure 5D**),
6
7 presumably due a cytotoxicity. In contrast, for compound **32** (**Figure 5E**) a significant
8
9 increase of differentiation was observed with respect to basal control at concentrations of 6
10
11 μ M ($p \leq 0.05$) and 8 μ M ($p \leq 0.01$, Mann-Whitney test), and for compound **42** (**Figure 5G**) at 5
12
13 μ M ($p \leq 0.05$, Mann-Whitney test). Thus, compounds **32** and **42** promote the differentiation
14
15 of CG4 cells into mature oligodendrocytes. In view of their pharmacological and biological
16
17 profiles, compounds **32** and **42** appear particularly suitable. Compounds **32** and **42** were also
18
19 evaluated on primary cultures of rat OPCs (**Figure 6**). In this model, the differentiation rate
20
21 was measured by the quantification of the number of MBP-expressing oligodendrocytes.
22
23 MBP is a major constituent of myelin and is commonly used as a marker of mature
24
25 oligodendrocytes. Compounds **32** and **42** promote the differentiation at concentrations of 8
26
27 μ M and 5 μ M, respectively. Overall, these findings support the pro-myelinating potential of
28
29 *para*-aminobenzyl-hit derivatives.
30
31
32
33
34
35
36
37
38
39
40
41
42
43
44
45
46
47
48
49
50
51
52
53
54
55
56
57
58
59
60

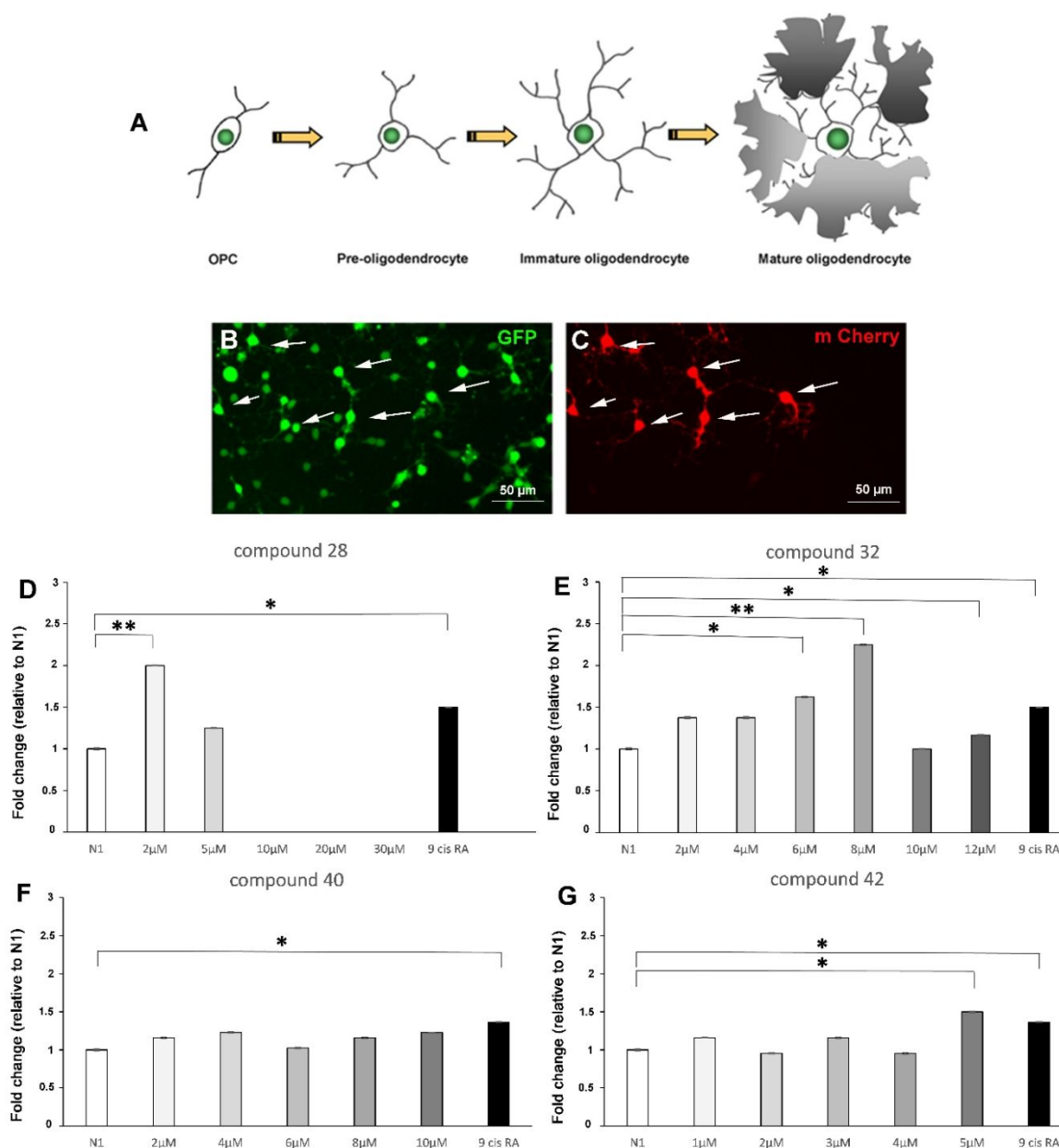


Figure 5: KLK6 inhibitors promote oligodendrocyte differentiation on the CG4 mCherry/GFP cell line.

Schematic representation of the different developmental stages of the CG4 cell line (A). Differentiation of the mCherry/GFP double fluorescent CG4 cell line, after 4 days of differentiation in basal medium (B-C). GFP fluorescence is shown in (B) and mCherry fluorescence in (C). Note that the differentiation of CG4 cells is not synchronous in these cultures and the expression of mCherry occurs specifically at the mature oligodendrocyte stage. Graphs of the fold change of the number of mCherry+ cells in N1 alone, N1 + compound **28** (D), N1 + compound **32** (E), N1 + compound **40** (F) or N1 + compound **42** (G), after 4 days of differentiation. The treatment with KLK6 inhibitors **32** and **42** induces a significant increase of CG4 cell differentiation at 8 μM and 5 μM respectively, relative to the N1 basal medium. Note that CG4 cells treated with compound **28** at 2 μM lead to a significant increase of the number of mCherry+ oligodendrocytes. However, at higher concentrations with this compound (ranging from 10 to 30 μM), cells were lost presumably due to a cytotoxicity. Wilcoxon - Mann Whitney test: * $p \leq 0.05$, ** $p \leq 0.01$. 9 cis retinoic acid (9cis-RA, 1 μM) was used as a positive control. Scale bar (B, C): 50 μm.

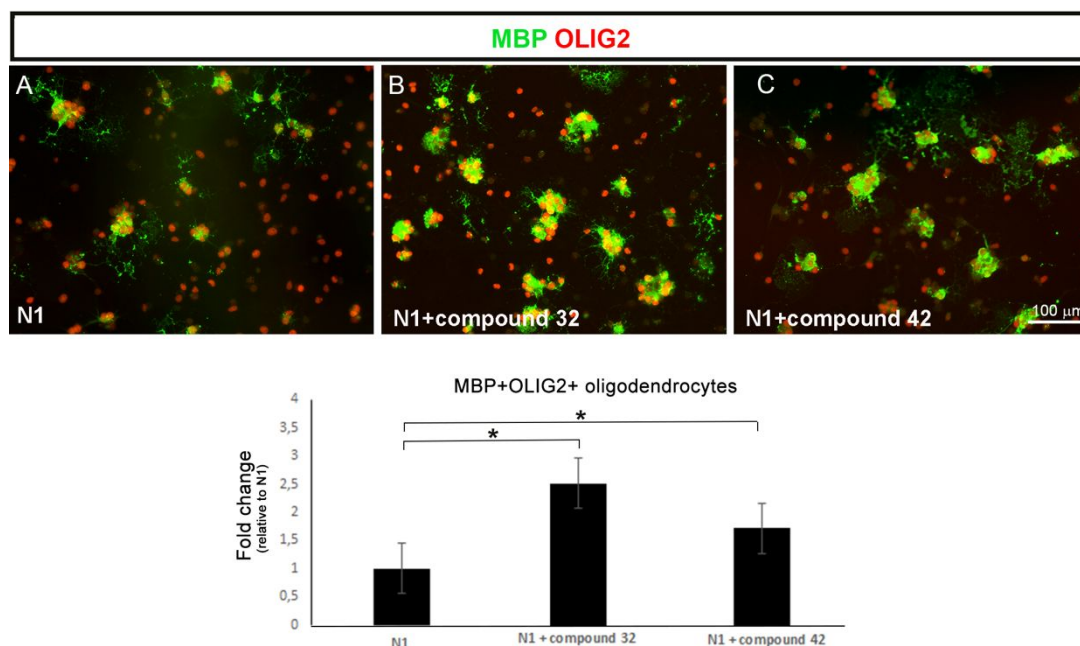


Figure 6: KLK6 inhibitors promote oligodendrocyte differentiation of primary OPC cultures. Primary OPC cultures, stained for MBP (green) and Olig2 (red), after 4 days of differentiation in basal medium (A), in the presence of compound **42** (B, 5 μ M) or compound **32** (C, 8 μ M). The treatment with KLK6 inhibitors induces a significant increase of MBP+ oligodendrocytes with respect to control. N=3 independent experiments; Wilcoxon - Mann Whitney test: * $p \leq 0.05$). Scale bar (A, B, C): 100 μ m.

Anti-inflammatory properties of hit compounds

In MS, chronic activation of microglia may contribute to neurodegeneration and neuroinflammation.³⁵ Thus, we also examined the impact of hit compounds **32** and **42** on microglial activation and pro-inflammatory cytokines. These experiments were carried in primary microglial cells isolated from newborn rat brain.³⁶ Effects of selected compounds on microglia were analyzed after treatment with lipopolysaccharide (LPS, 10 ng/ml) alone or in presence of different concentrations framing IC₅₀ values of compounds **32** and **42**, using dexamethasone as positive control (**Figure 7**). Using quantitative RT-qPCR of pro- and anti-inflammatory cytokine gene expression, we showed that compound **42** significantly lowered the expression of TNF α and IL1 β pro-inflammatory cytokines while compound **32** had no

effect. This result illustrates potential distinct dual therapeutical effects and/or mechanism of action for these hit compounds.

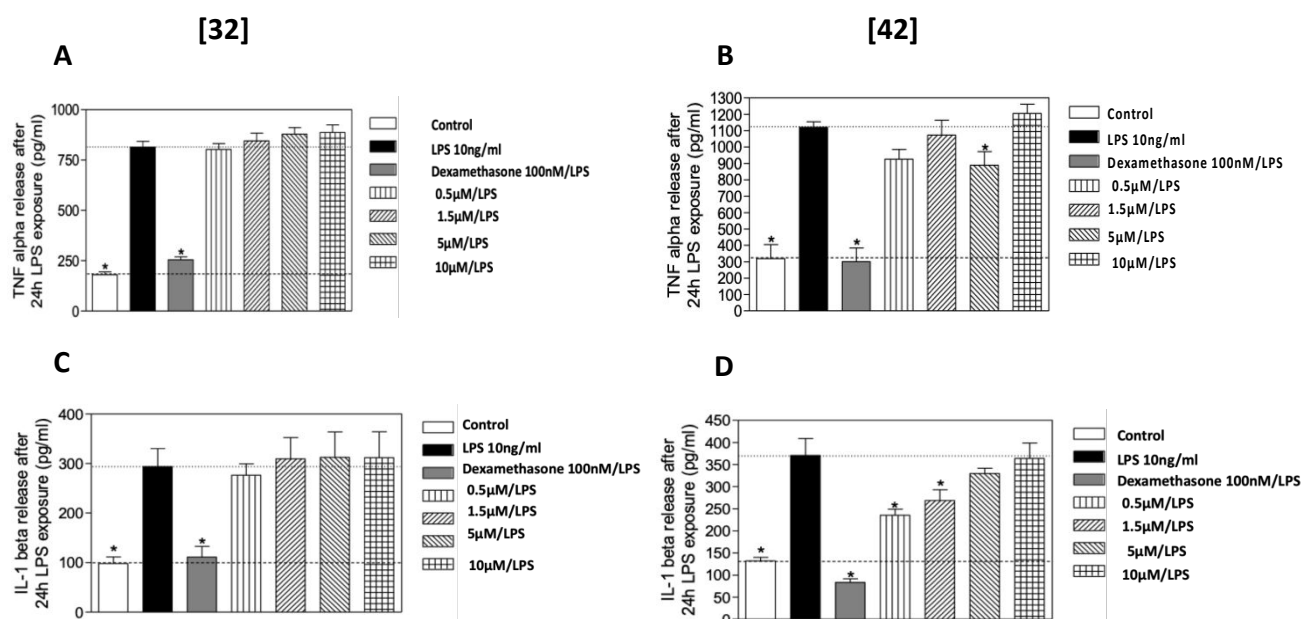


Figure 7: Anti-inflammatory potential of KLK6 inhibitors on a primary culture of microglia. Changes in TNF- α (A-B) and IL-1 β (C-D) secretions after 24 hours of LPS exposure (10 ng. mL⁻¹) and treatment by either inhibitor **32** (left) or **42** (right) in the concentration range [0,5 μ M – 10 μ M]. Cytokine secretion was measured by ELISA assay. The treatment with inhibitor **42** induces a significant decrease of TNF α and IL1- β secretions. Control: No treatment. Dexamethasone (100 nM): positive control (n=3). (graph, * p<0.05)

Molecular docking modelling to study structural basis of the inhibition

In silico analyzes using molecular docking with the AutoDock Vina software highlighted some characteristic structural bases on the inhibition of hit compounds **42** and **32** (Figure 8A). Figures 8B and 8C illustrates their positioning for the best docking poses. Overall, the orientation of both compounds within the active site is identical with the benzylamine group pointing to the S1 pocket and the phenol/naphthol groups to the catalytic triad. Inhibitors **32** (Figure 8B) and **42** (Figure 8A) share several polar contacts with some active site residues, namely H57 and S195. In particular, the NH of the amide bond of compound **32** establishes a

1
2
3 direct H-bond with the catalytic S195. We do not exclude a certain flexibility in this region,
4
5 given the obtained results, which could allow the NH of the amide bond of compound **42** to
6
7 behave similarly, this behavior may in part explain the non-competitive mechanism
8
9 underlined by Dixon plots. The OH hydroxyl group of phenols or naphthols could also
10
11 contribute to a polar bond with Q192 side chain as well as the NH backbone of G193. Finally,
12
13 the primary amine shows strong polar contact in both cases with D189 and S190 side chains
14
15 and with W215 backbone. The visual inspection of other docking poses with lower scores
16
17 informed us about the certain degree of freedom of the benzylamine moiety inside the S1
18
19 pocket, the benzyl group having enough space to slightly rotate around its axis, even
20
21 suggested by the two best poses of compounds **32** and **42**. These poses are quite compatible
22
23 with their mechanism of inhibition.
24
25
26
27
28
29
30
31
32
33
34
35
36
37
38
39
40
41
42
43
44
45
46
47
48
49
50
51
52
53
54
55
56
57
58
59
60

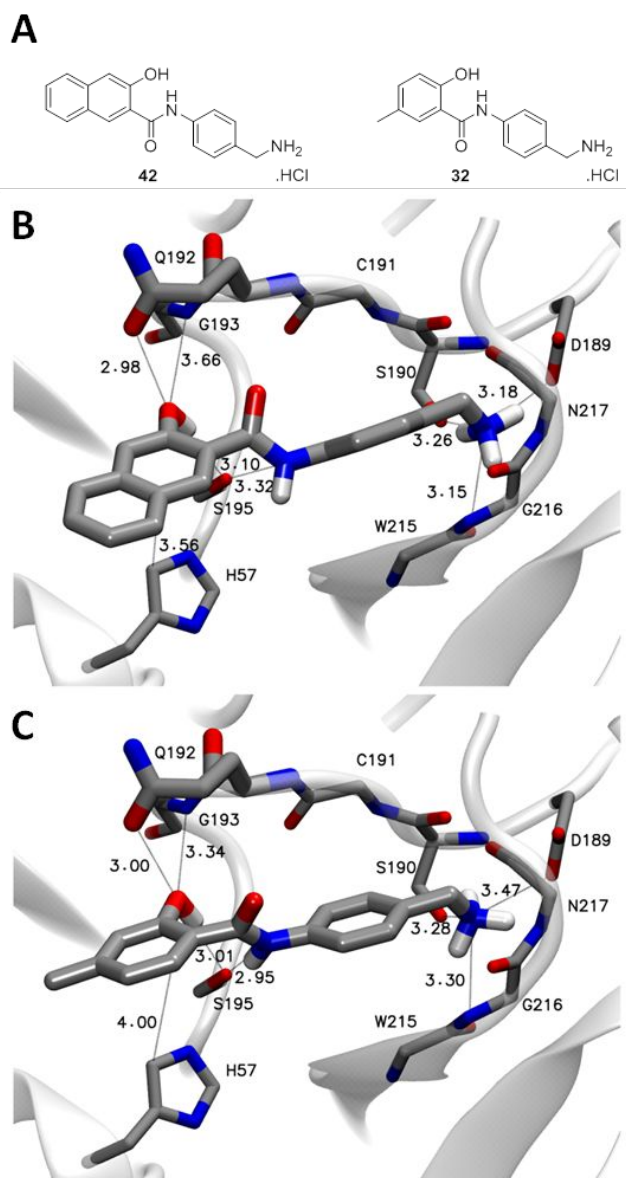


Figure 8: Structure of lead compounds **42** and **32** (A) and pose predictions by molecular docking of **42** (B) and **32** (C) in KLK6. Most relevant interactions were depicted by dashed lines together with distances in Angström. Compounds as well as residues of the proteins mainly involved in ligand interactions are shown in licorice while the full proteins are shown in transparent-white cartoon. The color code for the atoms is as follows: Carbon in grey, Oxygen in red, Nitrogen in blue and Hydrogen in white. The side chains which make no contact with **42** and **32**, as well as hydrogens of the protein and non-polar hydrogens of **42** and **32** were not represented for clarity.

Pharmacological profile and evaluation of drug-like properties

To gain more insights on the drug-like potential of the two selected hit compounds, different evaluations were performed to assess their: i) their putative effect of on coagulation; iii) their cross-reactivity toward key pharmacological targets using the SafetyScreen44™ Panel from Eurofins ³⁷; iv) some ADME-Tox properties: solution properties (aqueous solubility in simulated fluids and plasma protein binding), *in vitro* absorption (Caco2 cell line); *in vitro* metabolism (intrinsic clearance using human liver microsomes). More relevant parameters are summarized in Supplementary Data, **Table S2**. Altogether, these evaluations demonstrated that hit compounds **32** and **42** bear a very favorable pharmacological profile. They were shown to have no toxicity on coagulation after incubation with human blood (neither the activated partial thromboplastin time nor the prothrombin ratio were modified) and to possess acceptable aqueous solubility (> 150 μM, except for **42** at pH ≥ 7.4), permeability (> 90%) and clearance properties (half-life >120 min) when compared to reference substances. Interestingly, among the 44 screened targets both receptors and enzymes, very few were inhibited by our lead compounds. No activity at ion channels (including hERG) was detected meaning weak toxicity. The only significant detected off targets were of interest both for CNS diseases (5-HT_{2A/2B} serotonin receptors) or inflammation (COX-2). ³⁸ Hence, the selected compounds display favorable drug-like properties and constitute thus excellent starting point to derive drugs for regenerative therapy of MS and related-diseases associated with a deregulation of KLK6 and proximal proteolytic network.

Conclusion

Current MS therapeutics are mainly immuno- modulatory, having very few effect on neuroregeneration of damaged CNS tissue; they are thus primarily effective at the acute stage of disease, but much less so at the chronic stage. An MS therapy that has both immunomodulatory and neuro- regenerative effects would be highly beneficial. Novel targets aiming to promote such therapeutic strategies are thus of great interest. ⁸ KLK6 and its proximal proteolytic network may constitute a new opportunity to develop new therapeutics or molecular tools for MS pathophysiology. A series of *para*-aminobenzyl derivatives incorporating a phenol or a naphthol group was thus designed, synthesized and studied for their properties to inhibit KLK6 activity and proteases that may be involved into the KLK6's pathological network in MS, namely inhibitions of both KLK1 and plasmin may be interesting in a polypharmacological perspective.

Several designed low molecular weight inhibitors are low-micromolar potency and reversible towards KLK6. In the phenol series, introduction of an alkyl group at the C4 position led to more potent compounds (**32** and **37**), whereas in the naphthol series, the best activity was obtained with the 1- and 3-naphthol derivatives (**40** and **42**). Interestingly, these hit compounds were selective of KLK6 and its associated network over a large set of CNS concurrent proteases, and devoid of cytotoxic effects on primary cultures of mouse cortical and striatal neurons and oligodendrocytes. Most importantly, we show for the first time that synthetic inhibitors of KLK6 and proximal proteolytic network, a key actor of MS pathophysiology, are able to promote the differentiation of OPCs into mature oligodendrocytes *in vitro*, which is as far as we know the first report of such properties. Indeed, the presence of oligodendrocyte progenitors (OPCs) in the adult CNS, which are able to migrate and regenerate remyelinating oligodendrocytes in demyelinating lesions, represent

1
2
3 the main cellular target for the development of pharmacological strategy aiming to promote
4 remyelination. In line with this idea, compounds **32** and **42** were also tested for their
5 potential effect on neuroinflammation using primary cultures of microglia. Compound **42**
6 decreased significantly the expression of pro-inflammatory cytokines. Hence, compound **42**
7
8 in contrast to compound **32** appears to be a good candidate as a first-in-class KLK6 inhibitor
9
10 bearing both remyelinating and anti-inflammatory potentials. There is a growing
11 interest to decipher mechanisms regulating OPC differentiation for the
12 identification of novel specific pharmacological targets for remyelination-enhancing
13 therapy.³⁴ In another hand, there also a growing interest for pro-differentiating
14 compounds selected first through screening campaigns and more recently using
15 rational design as illustrated in up-to-date reports. Namely, spiroindolines were shown
16 as novel inducers of OPC differentiation.³⁹ Recently, benzothiazoles LRRK2 inhibitors
17 were shown to promote OPC proliferation and differentiation through Wnt/ β -catenin
18 signaling pathway.⁴⁰ Moreover, modified flavonoids were reported as selective inhibitors
19 of hyaluronidase activity and could promote OPC maturation, making them excellent
20 candidates to accelerate myelination or promote remyelination following perinatal and
21 adult CNS insults.⁴¹ Thus, in view of their pharmacological and biological properties,
22 *para*-aminobenzylamine derivatives **32** and **42** appear particularly valuable starting
23 points for the development of original pharmacological strategies aiming to promote
24 remyelination in demyelinating diseases, such as MS.
25
26
27
28
29
30
31
32
33
34
35
36
37
38
39
40
41
42
43
44
45
46
47
48
49
50
51
52
53
54
55
56
57
58
59
60

Experimental section

All reagents were analytical grade. Distilled water was filtered and deionized through a Millipore water purification system.

Chemistry Materials and General Procedures

Commercially available reagents and solvents were used without further purification.

Reactions were monitored by an analytical Waters Alliance 2690 HPLC instrument, equipped with a photodiode array and an analytical Chromolith Speed Rod RP-C18 185 Pm column (50 x 4.6 mm, 5 mm), at a flow rate of 3.0 mL/min, and gradients of 100/0 to 0/100 eluents A/B for 5 min (eluent A = H₂O/0.1% TFA and B = CH₃CN/0.1% TFA). Detection was performed at 214 nm. ¹H and ¹³C NMR spectra were recorded on Bruker spectrometers (300 or 400 MHz) at room temperature in deuterated solvents. Chemical shifts (δ) are expressed in parts per million (ppm), relative to the resonance of CDCl₃ = 7.26 ppm for ¹H (77.16 ppm for ¹³C), CD₃OD = 3.31 ppm for ¹H (49.00 ppm for ¹³C) or DMSO d₆ = 2.50 ppm for ¹H (39.52 ppm for ¹³C). The following abbreviations were used: s (singlet), d (doublet), t (triplet), q (quartet), m (multiplet), bs (broad singlet). Analytical thin-layer chromatography (TLC) was carried out on aluminum plates covered with 0.2 mm of silica and column chromatography was performed on silica gel 60 (70-230 mesh).

The LC/MS system consisted of a Waters Alliance 2695 HPLC, coupled to a Micromass (Manchester, UK) ZQ spectrometer (positive electrospray ionization mode, ESI+). All the analyses were carried out using a Merck Chromolith Speed rod C18, 25 x 4.6 mm reversed-phase column. A flow rate of 3mL/min and a gradient of (0–100) % B over 3 min (or over 15 min) were used. Eluent A: water/0.1% HCO₂H; eluent B: acetonitrile/0.1% HCO₂H. Retention

1
2
3 times (RT) are given in minutes. Nitrogen was used for both the nebulizing and drying gas. The
4
5 data were obtained in a scan mode ranging from 100 to 1000 m/z in 0.1 s intervals; 10 scans
6
7 were summed up to get the final spectrum. High-resolution mass spectrometry analyses were
8
9 performed with a Waters Synapt G2-S time-of-flight mass spectrometer fitted with an
10
11 electrospray ionisation source. All measurements were performed in the positive ion mode.
12
13 Melting points (Mp) are uncorrected and were recorded on a Stuart capillary melting point
14
15 apparatus SMP3. All compounds tested for biological activity showed >95% purity, as assessed
16
17 by RP-HPLC (Chromolith Speed Rod RP-C18 185 Pm column 50 × 4.6 mm, 5 μm; flow rate: 5.0
18
19 mL/min; gradients from 100/0 to 0/100 eluents A/B over 5 min, in which eluent A = H₂O/0.1%
20
21 TFA and B = CH₃CN/0.1% TFA; detection was done at 214 nm).
22
23
24
25
26
27

28 Compound **26** was synthesized according to the procedure described by Darensburg et al.⁴²
29
30 and its physical characteristics were in agreement with the published data. Carboxylic acids
31
32 were commercially available or synthesized according to the procedures described in ESI.
33
34
35

36 37 **Synthesis of *tert*-butyl (4-nitrobenzyl) carbamate (**1**):**

38
39
40 To a solution of 4-nitrobenzylamine hydrochloride (1 g, 5.3 mmol) in 10 mL of
41
42 dichloromethane were added 480 μL of triethylamine (348 mg, 3.44 mmol, 1.3 equiv.) and
43
44 790 μL of *tert*-butyl dicarbonate (751 mg, 3.44 mmol, 1.3 equiv.). The solution was stirred at
45
46 room temperature for 2 hours. Then was added 0.3 equiv. of aminomethyl polystyrene resin
47
48 and the suspension was stirred for 1 hour. After filtration, the solution was washed with 1M
49
50 aqueous potassium hydrogensulfate solution (2x 15 mL) and with brine (15 mL). The organic
51
52 layer was dried over Na₂SO₄, filtered and the solvent is evaporated *in vacuo* to offer compound
53
54
55 **1** as a white solid (m= 1.06 g, 80% yield); mp 109-111°C (lit. 109-110°C)⁴³; ¹H NMR (CDCl₃, 300
56
57 MHz): δ ppm 1.43 (s, 9H), 4.37 (d, 2H, *J* = 6.2 Hz), 5.03 (bs, 1H), 7.41 (d, 2H, *J* = 8.8 Hz), 8.14 (d,
58
59
60

1
2
3 2H, $J = 8.8$ Hz); ^{13}C NMR (CDCl_3 , 75 MHz): δ ppm 27.5, 44.2, 85.3, 123.9, 127.9, 146.9, 147.4,
4
5 156.0; HPLC, RT= 1.68 min.
6
7

8 9 **Synthesis of *tert*-butyl (4-aminobenzyl)carbamate (2):**

10
11
12 To a solution of compound **1** (1 g, 4.0 mmol) in 20 mL of ethyl acetate was added 10%
13
14 palladium activated on charcoal (~20 mg). The suspension was hydrogenated at atmospheric
15
16 pressure for 4 hours at room temperature. The suspension was then filtered on celite and the
17
18 filtrate was evaporated under reduce pressure to yield compound **2** as a pale orange solid, m
19
20 = 880 mg, quantitative yield. Mp 72-75°C (lit. 72-75°C)⁴⁴; ^1H NMR (CDCl_3 , 300 MHz): δ ppm
21
22 1.43 (s, 9H), 3.60 (bs, 2H), 4.14 (d, 2H, $J = 5.6$ Hz), 4.74 (bs, 1H), 6.60 (d, 2H, $J = 8.4$ Hz), 7.02
23
24 (d, 2H, $J = 8.4$ Hz); ^{13}C NMR (CDCl_3 , 75 MHz): δ ppm 28.5, 44.5, 79.4, 115.3, 128.9, 135.1, 145.8,
25
26 155.9; HPLC, RT= 0.93 min; MS (ESI+): m/z 223.3 $[\text{M}+\text{H}]^+$.
27
28
29
30
31
32

33 **General procedure for the synthesis of compounds 3-28:**

34
35
36 To a solution of 100 mg of compound **2** (0.45 mmol) in 2.5 mL of THF was added 1 equiv. of
37
38 the appropriate carboxylic acid derivative (0.45 mmol) and 103 mg of *N*-(3-
39
40 dimethylaminopropyl)-*N'*-ethylcarbodiimide hydrochloride (1 equiv., 0.45 mmol). The
41
42 solution was stirred at reflux for 12 hours. After cooling to room temperature, the solution
43
44 was evaporated to dryness. The crude product was dissolved in 20 mL of ethyl acetate and the
45
46 solution was washed with 1N hydrochloric acid solution (3x20mL) and then by 10% aqueous
47
48 sodium carbonate solution. The organic layer was dried over Na_2SO_4 , filtered and the solvent
49
50 is evaporated *in vacuo*. The resulting crude mixture was washed with Et_2O for compounds **4**,
51
52 **10** and **23**. Compounds **13**, **16-21** and **24** were used without further purification in the
53
54 subsequent step. Other compounds were purified by chromatography on silica gel.
55
56
57
58
59
60

1
2
3 *Tert*-butyl (4-(5-*tert*-butyl-2-hydroxybenzoyl))aminobenzylcarbamate (**3**). Elution : DCM/EtOH
4
5 98.5/1.5 v/v; White solid (m= 58 mg, 32% yield); mp: 177-178°C; ¹H NMR (CDCl₃, 300 MHz): δ
6
7 ppm 1.31 (s, 9H), 1.44 (s, 9H), 4.26 (d, 2H, *J* = 5.9 Hz), 4.89 (bs, 1H), 6.93 (d, 1H, *J* = 8.7 Hz),
8
9 7.24 (m, 2H), 7.48 (m, 4H), 8.24 (bs, 1H), 11.0 (s, 1H); ¹³C NMR (CDCl₃, 75 MHz): δ ppm 28.6,
10
11 31.4, 31.6, 44.4, 79.9, 114.4, 118.4, 121.9, 122.1, 128.2, 132.3, 136.0, 136.1, 142.0, 156.1,
12
13 159.3, 168.7; HPLC, RT= 2.10 min; MS (ESI+): *m/z* 399.3 [M+H]⁺; HRMS calcd for C₂₃H₃₁N₂O₄
14
15 399.2278, found 399.2272.
16
17
18
19
20

21 *Tert*-butyl (4-(2-hydroxybenzoyl))aminobenzylcarbamate (**4**). White solid (m= 113 mg, 73%
22
23 yield); mp: 107-171°C; ¹H NMR (DMSO *d*₆, 300 MHz): δ ppm 1.40 (s, 9H), 3.30 (bs, 1H), 4.10 (d,
24
25 2H, *J* = 6.0 Hz), 6.96 (m, 2H), 7.23 (d, 2H, *J* = 8.4 Hz), 7.33 (bt, 1H, *J* = 6.0 Hz), 7.44 (td, 1H, *J* =
26
27 8.5 Hz, 1.6 Hz), 7.62 (d, 2H, *J* = 8.4 Hz), 7.97 (dd, 1H, *J* = 8.5 Hz, 1.6 Hz), 10.35 (s, 1H); ¹³C NMR
28
29 (DMSO *d*₆, 75 MHz): δ ppm 28.2, 43.0, 77.7, 117.2, 118.9, 120.9, 127.3, 128.9, 133.6, 136.0,
30
31 136.6, 155.7, 158.6, 166.5; HPLC, RT= 1.78 min; MS (ESI+): *m/z* 365.0 [M+Na]⁺, 287.1 [M+H-
32
33 *t*Bu]⁺; HRMS calcd for C₁₉H₂₃N₂O₄ 343.1652, found 343.1655.
34
35
36
37
38
39

40 *Tert*-butyl (4-(3-methyl-2-hydroxybenzoyl))aminobenzylcarbamate (**5**). Elution: DCM/EtOH
41
42 92/2 v/v. Light yellow solid (m= 125 mg, 78% yield); mp: 166.2-166.9°C; ¹H NMR (CDCl₃, 400
43
44 MHz): δ ppm 1.45 (s, 9H), 2.27 (s, 3H), 4.28 (d, 2H, *J* = 5.7 Hz), 4.85 (bs, 1H), 6.79 (t, 1H, *J* = 7.7
45
46 Hz), 7.28 (m, 3H), 7.37 (d, 1H, *J* = 7.7 Hz), 7.50 (d, 2H, *J* = 8.4 Hz), 8.00 (bs, 1H), 12.3 (s, 1H); ¹³C
47
48 NMR (CDCl₃, 100 MHz): δ ppm 16.0, 28.6, 44.4, 79.9, 113.8, 118.4, 121.7, 123.1, 128.3, 128.4,
49
50 135.6, 136.1, 136.2, 156.1, 160.5, 169.1; HPLC, RT= 2.01 min; MS (ESI+): *m/z* 379.2 [M+Na]⁺,
51
52 301.2 [M+H-*t*Bu]⁺; HRMS calcd for C₂₀H₂₅N₂O₄ 357.1809, found 357.1811.
53
54
55
56
57
58
59
60

1
2
3 *Tert*-butyl (4-(4-methyl-2-hydroxybenzoyl))aminobenzylcarbamate (**6**). Elution: *n*-Hex/AcOEt
4
5 2/1 v/v. Light yellow solid (m= 131 mg, 82% yield); mp: 191.8-192.8°C; ¹H NMR (CDCl₃, 400
6
7 MHz): δ ppm 1.45 (s, 9H), 2.33 (s, 3H), 4.28 (d, 2H, *J* = 5.5 Hz), 4.84 (bs, 1H), 6.70 (dd, 1H, *J* =
8
9 8.1 Hz, 1.1 Hz), 6.82 (d, 1H, *J* = 1.1 Hz), 7.27 (d, 2H, *J* = 8.4 Hz), 7.39 (d, 1H, *J* = 8.1 Hz), 7.50 (d,
10
11 2H, *J* = 8.4 Hz), 7.93 (bs, 1H), 11.94 (s, 1H); ¹³C NMR (CDCl₃, 100 MHz): δ ppm 21.9, 28.6, 44.4,
12
13 79.9, 112.1, 119.3, 120.3, 121.6, 125.5, 128.4, 136.1, 136.2, 146.1, 156.1, 162.1, 168.6; HPLC,
14
15 RT= 1.90 min; MS (ESI+): *m/z* 357.2 [M+H]⁺, 379.1 [M+Na]⁺, 301.2 [M+H-*t*Bu]⁺; HRMS calcd for
16
17 C₂₀H₂₅N₂O₄ 357.1809, found 357.1809.
18
19
20
21
22

23
24 *Tert*-butyl (4-(5-methyl-2-hydroxybenzoyl))aminobenzylcarbamate (**7**). Elution: *n*-Hex/AcOEt
25
26 2/1 v/v. Light yellow solid (m= 68 mg, 42% yield); mp: 174.5-175.5°C; ¹H NMR (CDCl₃, 400
27
28 MHz): δ ppm 1.45 (s, 9H), 2.32 (s, 3H), 4.28 (d, 2H, *J* = 5.4 Hz), 4.84 (bs, 1H), 6.91 (d, 1H, *J* = 8.4
29
30 Hz), 7.22-7.29 (m, 4H), 7.52 (d, 2H, *J* = 8.4 Hz), 7.96 (bs, 1H), 11.71 (s, 1H); ¹³C NMR (CDCl₃, 100
31
32 MHz): δ ppm 20.8, 28.6, 44.4, 79.9, 114.4, 115.5, 118.8, 121.6, 123.3, 125.7, 128.4, 135.8,
33
34 136.1, 156.1, 159.8, 168.6; HPLC, RT= 1.90 min; MS (ESI+): *m/z* 379.2 [M+Na]⁺, 301.2 [M+H-
35
36 *t*Bu]⁺; HRMS calcd for C₂₀H₂₅N₂O₄ 357.1809, found 357.1810.
37
38
39
40

41
42 *Tert*-butyl (4-(6-methyl-2-hydroxybenzoyl))aminobenzylcarbamate (**8**). Elution: *n*-Hex/AcOEt
43
44 2/1 v/v. Light yellow solid (m= 33 mg, 21% yield); mp: 149.0-150.0°C; ¹H NMR (CDCl₃, 300
45
46 MHz): δ ppm 1.46 (s, 9H), 2.60 (s, 3H), 4.28 (d, 2H, *J* = 5.4 Hz), 4.91 (bs, 1H), 6.76 (d, 1H, *J* = 7.5
47
48 Hz), 6.84 (d, 1H, *J* = 8.2 Hz), 7.23 (dd, 1H, *J* = 8.2 Hz, 7.5 Hz), 7.27 (d, 2H, *J* = 8.0 Hz), 7.52 (d,
49
50 2H, *J* = 8.0 Hz), 7.72 (s, 1H), 9.85 (bs, 1H); ¹³C NMR (CDCl₃, 75 MHz): δ ppm 22.1, 28.5, 44.3,
51
52 78.3, 115.7, 119.0, 121.0, 123.1, 128.4, 132.5, 135.5, 136.1, 136.2, 156.1, 159.2, 168.4; HPLC,
53
54 RT= 1.60 min; MS (ESI+): *m/z* 379.1 [M+Na]⁺, 301.2 [M+H-*t*Bu]⁺; HRMS calcd for C₂₀H₂₅N₂O₄
55
56 357.1809, found 357.1808.
57
58
59
60

1
2
3 *Tert*-butyl (4-(5-bromo-2-hydroxybenzoyl))aminobenzylcarbamate (**9**). Elution: *n*-Hex/AcOEt
4
5 4/1 v/v. White solid (m= 24 mg, 12% yield); mp: >300°C ¹H NMR (DMSO *d*₆, 400 MHz): δ ppm
6
7 1.93 (s, 9H), 4.10 (d, 2H, *J* = 6.0 Hz), 6.95 (d, 1H, *J* = 8.8 Hz), 7.23 (d, 2H, *J* = 8.3 Hz), 7.37 (t, 1H,
8
9 *J* = 6.8 Hz), 7.57 (dd, 1H, *J* = 8.8 Hz, 2.6 Hz), 7.62 (d, 2H, *J* = 8.3 Hz), 8.08 (d, 1H, *J* = 2.6 Hz),
10
11 10.44 (s, 1H), 11.93 (bs, 1H); ¹³C NMR (CDCl₃, 100 MHz): δ ppm 28.2, 43.0, 77.8, 110.0, 119.6,
12
13 119.9, 120.8, 127.3, 131.1, 135.8, 136.2, 136.5, 155.8, 157.6, 164.9; HPLC, RT= 2.00 min; MS
14
15 (ESI+): *m/z* 443.0 [M+Na]⁺, 445.0 [M+2+Na]⁺, 367.0 [M+H-tBu]⁺, 365.0 [M+H+2-tBu]⁺; HRMS
16
17 calcd for C₁₉H₂₁BrN₂NaO₄ 443.0577, found 443.0575.
18
19
20
21
22
23

24 *Tert*-butyl (4-(5-methoxy-2-hydroxybenzoyl))aminobenzylcarbamate (**10**). White solid (m= 75
25
26 mg, 45% yield); ¹H NMR (DMSO *d*₆, 300 MHz): δ ppm 1.39 (s, 9H), 3.76 (s, 3H), 4.10 (d, 2H, *J* =
27
28 5.9 Hz), 6.92 (d, 1H, *J* = 8.9 Hz), 7.06 (ddd, 1H, *J* = 9.0 Hz, 9.0 Hz, 3.0 Hz), 7.23 (d, 2H, *J* = 8.3
29
30 Hz), 7.37 (bt, 1H, *J* = 5.9 Hz), 7.50 (d, 1H, *J* = 3.0 Hz), 7.62 (d, 2H, *J* = 8.3 Hz), 10.90 (s, 1H); ¹³C
31
32 NMR (DMSO *d*₆, 75 MHz): δ ppm 28.2, 43.0, 55.7, 77.8, 112.5, 117.3, 118.1, 120.6, 121.0,
33
34 127.4, 136.1, 136.6, 151.8, 152.3, 155.8, 166.0; ; HPLC, RT= 1.78 min; MS (ESI+): *m/z* 395.1
35
36 [M+Na]⁺, 373.1 [M+H]⁺; 317.1 [M+H-tBu]⁺.
37
38
39
40
41

42 *Tert*-butyl (4-(4-isopropyl-2-hydroxybenzoyl))aminobenzylcarbamate (**11**). Elution: *n*-
43
44 Hex/AcOEt 3/1 v/v. White solid (m= 53 mg, 31% yield); ¹H NMR (CDCl₃, 400 MHz): δ ppm 1.60
45
46 (d, 6H, *J* = 6.7 Hz), 1.83 (s, 9H), 3.24 (hept., 1H, *J* = 6.7 Hz), 4.64 (d, 2H, *J* = 4.0 Hz), 5.25 (bs,
47
48 1H), 7.12 (d, 1H, *J* = 7.1 Hz), 7.60 (d, 2H, *J* = 7.6 Hz), 7.86 (m, 3H), 8.47 (bs, 1H), 12.30 (bs, 1H);
49
50 ¹³C NMR (CDCl₃, 100 MHz): δ ppm 23.7, 28.6, 34.4, 44.4, 79.9, 112.5, 116.5, 117.9, 121.7,
51
52 125.8, 128.3, 136.0, 136.2, 156.2, 156.9, 162.1, 168.6; HPLC, RT= 2.09 min; MS (ESI+): *m/z*
53
54 407.1 [M+Na]⁺, 385.2 [M+H]⁺.
55
56
57
58
59
60

1
2
3 *Tert*-butyl (4-(4-trifluoromethyl-2-hydroxybenzoyl))aminobenzylcarbamate (**12**). Elution
4
5 DCM/EtOH 99/1 v/v; White solid (m= 114 mg, 62% yield); mp: 179.5-180.5°C; ¹H NMR (CD₃OD,
6
7 400 MHz): δ ppm 1.46 (s, 9H), 4.22 (s, 2H), 4.76 (bs, 1H), 7.22 (m, 2H), 7.29 (d, 2H, *J* = 8.4 Hz),
8
9 7.63 (d, 2H, *J* = 8.4 Hz), 8.11 (d, 1H, *J* = 8.6 Hz); ¹³C NMR (CD₃OD, 100 MHz): δ ppm 28.8, 44.6,
10
11 80.2, 115.2 (d, *J* = 3.7 Hz), 116.5 (d, *J* = 3.7 Hz), 122.0, 122.5, 126.3, 128.7, 131.2, 135.8, 137.8,
12
13 158.6, 160.4, 165.2, 167.4 ; HPLC, RT= 1.86 min; MS (ESI+): *m/z* 433.0 [M+Na]⁺, 411.1 [M+H]⁺,
14
15 355.0 [M+H-tBu]⁺; HRMS calcd for C₂₀H₂₂F₃N₂O₄ 411.1526, found 411.1537.
16
17
18
19
20

21 *Tert*-butyl (4-(4-fluoro-2-hydroxybenzoyl))aminobenzylcarbamate (**13**). Elution DCM/EtOH
22
23 99/1 v/v; White solid (m= 37 mg, 23% yield); mp: 155-5-156.5°C; ¹H NMR (CD₃OD, 400 MHz):
24
25 δ ppm 1.45 (s, 9H), 4.21 (s, 2H), 6.64-6.70 (m, 2H), 7.26 (d, 2H, *J* = 8.4 Hz), 7.59 (d, 2H, *J* = 8.4
26
27 Hz), 7.98 (dd, 1H, *J* = 9.4 Hz, 8.4 Hz); ¹⁹F NMR (CD₃OD, 400 MHz): δ ppm -107.1; ¹³C NMR
28
29 (CD₃OD, 100 MHz): δ ppm 28.9, 44.8, 80.3, 105.2 (d, *J* = 24.2 Hz), 107.6 (d, *J* = 24.2 Hz), 114.8,
30
31 122.7, 128.8, 132.1 (d, *J* = 11.1 Hz), 132.5, 137.5, 138.0, 163.3 (d, *J* = 13.3 Hz), 167.4 (d, *J* =
32
33 251.3 Hz), 168.4; HPLC, RT= 1.88 min; MS (ESI+): *m/z* 383.1 [M+Na]⁺, 361.1 [M+H]⁺, 305.1
34
35 [M+H-tBu]⁺; HRMS calcd for C₁₉H₂₂FN₂O₄ 361.1558, found 361.1554.
36
37
38
39
40
41

42 *Tert*-butyl (4-(1-hydroxy-2-naphtoyl))aminobenzylcarbamate (**14**). Elution : *n*-Hex/AcOEt 3/1
43
44 v/v; White solid (m= 40 mg, 23% yield); mp: 145-146°C; ¹H NMR (DMSO *d*₆, 300 MHz): δ ppm
45
46 1.40 (s, 9H), 4.13 (d, 2H, *J* = 5.9 Hz), 7.27 (d, 2H, *J* = 8.1 Hz), 7.40 (bt, 1H, *J* = 5.9 Hz), 7.46 (d,
47
48 1H, *J* = 8.9 Hz), 7.58 (dd, 1H, *J* = 8.1 Hz, 7.1 Hz), 7.68 (m, 3H), 7.92 (d, 1H, *J* = 8.1 Hz), 8.10 (d,
49
50 1H, *J* = 9.0 Hz), 8.31 (d, 1H, *J* = 8.1 Hz), 10.92 (bs, 1H); ¹³C NMR (DMSO *d*₆, 75 MHz): δ ppm
51
52 28.2, 43.0, 77.8, 107.5, 117.7, 121.1, 123.0, 124.7, 125.9, 127.2, 127.5, 129.1, 136.0, 136.1,
53
54 136.7, 155.8, 160.0, 169.4; HPLC, RT= 2.13 min; MS (ESI+): *m/z* 415.1 [M+Na]⁺, 337.0 [M+H-
55
56 tBu]⁺; HRMS calcd for C₂₃H₂₅N₂O₄ 393.1809, found 393.1807.
57
58
59
60

1
2
3 *Tert*-butyl (4-(2-hydroxy-1-naphtoyl))aminobenzylcarbamate (**15**). Elution: DCM/EtOH
4
5 98.5/1.5 v/v; White solid (m= 90 mg, 51% yield); mp: 188.5-189.5°C; ¹H NMR (CDCl₃, 300 MHz):
6
7 δ ppm 1.45 (s, 9H), 4.28 (d, 2H, *J* = 5.6 Hz), 4.88 (bs, 1H), 7.16 (d, 1H, *J* = 9.0 Hz), 7.29 (d, 2H, *J*
8
9 = 8.8 Hz), 7.36 (dd, 1H, *J* = 7.4 Hz, 6.8 Hz), 7.54 (m, 3H), 7.81 (m, 2H), 8.01 (bs, 1H), 8.14 (d, 1H,
10
11 *J* = 8.6 Hz), 10.92 (bs, 1H) ; ¹³C NMR (CDCl₃, 75 MHz): δ ppm 28.6, 44.4, 79.9, 110.3, 119.5,
12
13 121.0, 122.6, 123.8, 128.4, 128.6, 129.0, 129.7, 130.7, 134.4, 136.2, 136.3, 156.0, 159.7, 168.5;
14
15 HPLC, RT= 1.74 min; MS (ESI+): *m/z* 415.1 [M+Na]⁺, 337.0 [M+H-*t*Bu]⁺; HRMS calcd for
16
17 C₂₃H₂₅N₂O₄ 393.1809, found 393.1801.
18
19
20
21
22
23

24 *Tert*-butyl (4-(3-hydroxy-2-naphtoyl))aminobenzylcarbamate (**16**). White solid (m= 56 mg,
25
26 32% yield); mp: 199-200°C; ¹H NMR (DMSO *d*₆, 400 MHz): δ ppm 1.40 (s, 9H), 4.11 (d, 2H, *J* =
27
28 6.1 Hz), 7.25 (d, 2H, *J* = 8.4 Hz), 7.32 (s, 1H), 7.35 (m, 2H), 7.50 (ddd, 1H, *J* = 8.4 Hz, *J* = 6.8 Hz,
29
30 *J* = 1.0 Hz), 7.69 (d, 2H, *J* = 8.4 Hz), 7.75 (d, 1H, *J* = 8.2 Hz), 7.92 (d, 1H, *J* = 8.2 Hz), 8.51 (s, 1H),
31
32 10.65 (bs, 1H); ¹³C NMR (DMSO *d*₆, 100 MHz): δ ppm 28.2, 43.0, 77.7, 110.6, 120.5, 121.6,
33
34 123.7, 125.7, 126.8, 127.4, 128.1, 128.7 130.4, 135.8, 135.9, 137.0, 154.0, 155.8, 165.6; HPLC,
35
36 RT= 1.99 min; MS (ESI+): *m/z* 415.2 [M+Na]⁺, 337.1 [M+H-*t*Bu]⁺; HRMS calcd for C₂₃H₂₅N₂O₄
37
38 393.1809, found 393.1810.
39
40
41
42
43
44

45 *Tert*-butyl (4-(2-naphtoyl))aminobenzylcarbamate (**17**). White solid (m= 61 mg, 36% yield);
46
47 mp: 182.5-183.5°C; ¹H NMR (CDCl₃, 400 MHz): δ ppm 1.45 (s, 9H), 4.28 (d, 2H, *J* = 5.3 Hz), 4.86
48
49 (bs, 1H), 7.28 (d, 2H, *J* = 8.4 Hz), 7.56 (m, 2H), 7.63 (d, 2H, *J* = 8.4 Hz), 7.91 (m, 4H), 8.03 (bs,
50
51 1H), 8.36 (s, 1H); ¹³C NMR (CDCl₃, 100 MHz): δ ppm 28.6, 44.5, 79.8, 120.7, 123.8, 127.2, 127.8,
52
53 128.0, 128.1, 128.5, 129.0, 129.2, 132.3, 132.8, 135.1, 135.4, 137.4, 156.1, 166.0; HPLC, RT=
54
55 1.91 min; MS (ESI+): *m/z* 377.1 [M+H]⁺, 399.1 [M+Na]⁺, 321.3 [M+H-*t*Bu]⁺; HRMS calcd for
56
57 C₂₃H₂₅N₂O₃ 377.1860, found 377.1855.
58
59
60

1
2
3 *Tert*-butyl (1*H*-2-indolylcarbonyl)aminobenzylcarbamate (**18**). White solid (m= 67 mg, 41%
4
5 yield); mp: 207-208°C; ¹H NMR (DMSO *d*₆, 400 MHz): δ ppm 1.40 (s, 9H), 4.10 (s, 2H), 7.06 (t,
6
7 1H, *J* = 7.5 Hz), 7.22 (m, 3H), 7.36 (bs, 1H), 7.40 (s, 1H), 7.46 (d, 1H, *J* = 8.3 Hz), 7.66 (d, 1H, *J* =
8
9 7.5 Hz), 7.72 (d, 2H, *J* = 8.3 Hz), 10.2 (bs, 1H), 11.76 (bs, 1H); ¹³C NMR (DMSO *d*₆, 100 MHz): δ
10
11 ppm 28.3, 40.0, 77.7, 103.8, 112.4, 119.8, 120.1, 121.7, 123.7, 127.0, 127.3, 131.6, 135.3,
12
13 136.9, 137.5, 155.7, 159.7; HPLC, RT= 1.82 min; MS (ESI+): *m/z* 388.2 [M+Na]⁺, 310.2 [M+H-
14
15 tBu]⁺; HRMS calcd for C₂₁H₂₄N₃O₃ 366.1812, found 366.1812.
16
17
18
19

20
21 *Tert*-butyl (4-[(4-oxo-1,4-dihydroquinolin-3-yl)carbonyl]aminobenzylcarbamate (**19**). White
22
23 solid (m= 48 mg, 27% yield); mp: 238-239°C; ¹H NMR (DMSO *d*₆, 400 MHz): δ ppm 1.40 (s, 9H),
24
25 4.08 (d, 2H, *J* = 6.0 Hz), 7.17 (d, 2H, *J* = 8.3 Hz), 7.24 (td, 1H, *J* = 8.1 Hz, 1.1 Hz), 7.33 (t, 1H, *J* =
26
27 6.1 Hz), 7.50 (td, 1H, *J* = 8.1 Hz, 1.5 Hz), 7.59 (d, 1H, *J* = 8.1 Hz), 7.66 (d, 2H, *J* = 8.3 Hz), 8.24
28
29 (dd, 1H, *J* = 8.1 Hz, 1.1 Hz), 8.87 (s, 1H), 13.64 (s, 1H); ¹³C NMR (DMSO *d*₆, 100 MHz): δ ppm
30
31 28.3, 43.1, 77.7, 108.6, 118.9, 122.2, 124.7, 126.7, 127.5, 127.6, 129.3, 133.5, 139.0, 149.3,
32
33 151.6, 155.8, 166.1, 174.0; HPLC, RT= 1.67 min; MS (ESI+): *m/z* 394.2 [M+H]⁺, 338.2 [M+H-
34
35 tBu]⁺; HRMS calcd for C₂₂H₂₄N₃O₄ 394.1761, found 394.1756.
36
37
38
39
40

41 *Tert*-butyl (4-(3-hydroxypyridin-2-yl))aminobenzylcarbamate (**20**). Light yellow solid (m = 30
42
43 mg, 19% yield); mp: 90-92°C; ¹H NMR (CDCl₃, 400 MHz): δ ppm 1.45 (s, 9H), 4.29 (d, 2H, *J* = 5.7
44
45 Hz), 7.30 (d, 2H, *J* = 8.4 Hz), 7.31-7.37 (m, 2H), 7.65 (d, 2H, *J* = 8.4 Hz), 8.06 (bs, 1H), 8.10 (dd,
46
47 1H, *J* = 4.1 Hz, 1.6 Hz), 9.90 (bs, 1H), 11.89 (s, 1H); HPLC, RT= 1.85 min; MS (ESI+): *m/z* 366.1
48
49 [M+Na]⁺.
50
51
52
53
54

55 *Tert*-butyl (4-(6-methoxy-1-hydroxy-2-naphthoyl))aminobenzylcarbamate (**21**). White solid
56
57 (m= 34 mg, 18% yield); mp: 205.8-206.3°C; ¹H NMR (CDCl₃, 300 MHz): δ ppm 1.48 (s, 9H), 3.94
58
59
60

1
2
3 (s, 3H), 4.30 (d, 2H, $J = 5.4$ Hz), 4.87 (bs, 1H), 7.07 (d, 1H, $J = 2.3$ Hz), 7.16 (dd, 1H, $J = 9.1$ Hz,
4 2.4 Hz), 7.20 (d, 1H, $J = 8.1$ Hz), 7.30 (d, 2H, $J = 8.3$ Hz), 7.44 (d, 1H, $J = 9.1$ Hz), 7.55 (d, 2H, $J =$
5 8.3 Hz), 7.98 (bs, 1H), 8.35 (d, 1H, $J = 9.1$ Hz); ^{13}C NMR (CDCl_3 , 75 MHz): δ ppm 28.6, 44.4, 55.5,
6 79.3, 105.4, 106.2, 117.6, 118.2, 121.0, 121.6, 121.7, 125.9, 128.4, 136.0, 136.2, 138.6, 142.7,
7 143.1, 160.6, 161.6; HPLC, RT= 2.14 min; MS (ESI+): m/z 445.2 $[\text{M}+\text{Na}]^+$, 367.1 $[\text{M}+\text{H}-\text{tBu}]^+$;
8 HRMS calcd for $\text{C}_{24}\text{H}_{27}\text{N}_2\text{O}_5$ 423.1914, found 423.1911.
9
10
11
12
13
14
15
16
17
18

19 *Tert*-butyl (4-(7-methoxy-1-hydroxy-2-naphtoyl))aminobenzylcarbamate (**22**). White solid
20 (m= 30 mg, 16% yield); ^1H NMR (CDCl_3 , 400 MHz) : δ ppm 1.40 (s, 9H), 3.89 (s, 3H), 4.24 (d, 2H,
21 $J = 5.4$ Hz), 4.81 (bs, 1H), 7.17-7.29 (m, 6H), 7.49 (d, 1H, $J = 8.3$ Hz), 7.60 (d, 1H, $J = 8.9$ Hz), 7.65
22 (d, 1H, $J = 2.4$ Hz), 7.98 (bs, 1H), 13.38 (s, 1H); ^{13}C NMR (CDCl_3 , 400 MHz) : δ ppm 28.6, 29.9,
23 44.4, 55.7, 79.9, 102.2, 107.4, 118.5, 118.6, 121.7, 122.0, 126.9, 128.5, 129.1, 131.9, 136.2,
24 156.1, 158.3, 160.3, 169.5; HPLC, RT= 2,12 min ; MS (ESI+) : m/z 423.1 $[\text{M}+\text{H}]^+$, m/z 845.3
25 $[\text{2M}+\text{H}]^+$, m/z 440.2 $[\text{M}+\text{NH}_4]^+$.
26
27
28
29
30
31
32
33
34
35
36

37 *Tert*-butyl (4-(7-methyl-1-hydroxy-2-naphtoyl))aminobenzylcarbamate (**23**). Elution: *n*-
38 Hex/AcOEt 4/1 v/v. White solid (m= 140 mg, 77% yield); mp: 188.3-188.9°C; ^1H NMR (CDCl_3 ,
39 500 MHz): δ ppm 1.41 (s, 9H), 2.47 (s, 3H), 4.22 (d, 2H, $J = 5.8$ Hz), 4.84 (bt, 1H), 7.20 (m, 3H),
40 7.34 (d, 1H, $J = 9.0$ Hz), 7.36 (dd, 1H, $J = 8.4$ Hz, 1.4 Hz), 7.46 (d, 1H, $J = 8.1$ Hz), 7.60 (d, 1H, $J =$
41 8.4 Hz), 8.05 (bs, 1H), 8.15 (s, 1H), 13.45 (s, 1H); ^{13}C NMR (CDCl_3 , 125 MHz): δ ppm 22.0, 28.6,
42 44.3, 79.9, 107.0, 118.5, 120.0, 121.8, 123.0, 125.9, 127.4, 128.4, 131.6, 134.8, 136.0, 136.1,
43 136.2, 156.1, 161.0, 169.5; HPLC, RT= 2.23 min; MS (ESI+): m/z 429.1 $[\text{M}+\text{Na}]^+$, 407.2 $[\text{M}+\text{H}]^+$,
44 351.1 $[\text{M}+\text{H}-\text{tBu}]^+$; HRMS calcd for $\text{C}_{24}\text{H}_{27}\text{N}_2\text{O}_4$ 407.1965, found 407.1962.
45
46
47
48
49
50
51
52
53
54
55
56
57
58
59
60

1
2
3 *Tert*-butyl (4-(7-chloro-1-hydroxy-2-naphtoyl))aminobenzylcarbamate (**24**). White solid (m=
4 101 mg, 53% yield); RMN ¹H (CDCl₃, 400 MHz): δ ppm 1.58 (s, 9H), 4.32 (d, 2H, *J* = 5.7 Hz), 4.88
5
6 (bs, 1H), 7.33 (m, 3H), 7.48 (d, 1H, *J* = 8.8 Hz), 7.55 (dd, 1H, *J* = 8.8 Hz, 2.2 Hz), 7.57 (d, 2H, *J* =
7
8 8.3 Hz), 7.72 (d, 1H, *J* = 8.7 Hz), 8.00 (s, 1H), 8.43 (d, 1H, *J* = 2.2 Hz), 13.51 (s, 1H); RMN ¹³C
9
10 (CDCl₃, 400 MHz): δ ppm 28.6, 44.4, 79.9, 107.7, 118.4, 121.1, 121.7, 123.4, 126.6, 128.5,
11
12 129.2, 130.2, 132.4, 134.7, 135.9, 136.4, 156.1, 160.6, 169.0; HPLC, RT= 2,12 min; MS (ESI+):
13
14 m/z 371.1 [M+H-*t*Bu]⁺, 373.1[M+H-*t*Bu+2]⁺, 444.1 [M+NH₄]⁺, 446.1 [M+NH₄+2]⁺, 427.1 [M+H]⁺,
15
16 429.1 [M+H+2]⁺.
17
18
19
20
21
22

23 *Tert*-butyl (4-(6,7-dimethoxy-1-hydroxy-2-naphtoyl))aminobenzylcarbamate (**25**). ELution:
24 nHex/AcOEt 2/1 v/v. White solid (m= 140 mg, 69% yield); ¹H NMR (CDCl₃, 400 MHz): δ ppm
25
26 1.47 (s, 9H), 4.02 (s, 3H), 4.04 (s, 3H), 4.31 (d, 2H, *J* = 5.4 Hz), 4.87 (bs, 1H), 7.07 (s, 1H), 7.18
27
28 (d, 1H, *J* = 8.7 Hz), 7.30 (d, 2H, *J* = 8.3 Hz), 7.36 (d, 1H, *J* = 8.8 Hz), 7.56 (d, 2H, *J* = 8.3 Hz), 7.70
29
30 (s, 1H), 8.01 (s, 1H), 13.44 (s, 1H); ¹³C NMR (CDCl₃, 100 MHz): δ ppm 28.6, 44.4, 56.2, 56.3,
31
32 79.8, 102.9, 106.1, 106.5, 117.3, 119.5, 120.7, 121.7, 128.5, 131.1, 133.0, 136.0, 136.3, 149.6,
33
34 152.1, 160.2, 169.5; HPLC, RT= 3.81 min; MS (ESI+): m/z 397.2 [M+H-*t*Bu]⁺, 453.3[M+H]⁺, 475.3
35
36 [M+Na]⁺.
37
38
39
40
41
42
43
44

45 **Synthesis of *tert*-butyl (4-(5-*tert*-butyl-2-hydroxybenzyl)amino)benzyl)carbamate (**29**).**

46
47
48 To a solution of 100 mg of compound **2** (0.45 mmol) in 2.5 mL of ethanol were added 80 mg
49
50 of aldehyde **26** (0.45 mmol, 1 equiv.). The solution was stirred at reflux for 6 hours. After
51
52 cooling to room temperature, were added 9 mg of sodium borohydride (0.235 mmol, 0.5
53
54 equiv.) and the solution was stirred at room temperature for 1h30. Then, 20 mL of water were
55
56 added and the solution was extracted with ethyl acetate (3x20 mL). The organic layer was
57
58
59
60

1
2
3 dried over Na_2SO_4 , filtered and the solvent is evaporated *in vacuo* to offer compound **30** as a
4 white solid (m= 110 mg, 64% yield); mp 102.0-103.0°C; ^1H NMR (CDCl_3 , 300 MHz): δ ppm 1.29
5
6 (s, 9H), 1.44 (s, 9H), 4.19 (d, 2H, $J = 5.6$ Hz), 4.35 (s, 2H), 4.81 (bs, 2H), 6.76 (d, 2H, $J = 8.4$ Hz),
7
8 6.81 (d, 1H), 7.12 (m, 3H), 7.21 (dd, 1H, $J = 8.4$ Hz, 2.4 Hz), 11.2 (s, 1H); ^{13}C NMR (CDCl_3 , 75
9
10 MHz): δ ppm 28.6, 31.7, 44.4, 48.8, 64.9, 79.6, 115.8, 116.1, 122.4, 124.9, 125.8, 126.1, 128.8,
11
12 130.9, 143.0, 146.9, 154.2; HPLC, RT= 3.57 min; MS (ESI+): m/z 329.1 $[\text{M}+\text{H}-\text{tBu}]^+$, 385.1
13
14 $[\text{M}+\text{H}]^+$, 407.1 $[\text{M}+\text{Na}]^+$; HRMS calcd for $\text{C}_{23}\text{H}_{33}\text{N}_2\text{O}_3$ 385.2486, found 385.2499.
15
16
17
18
19
20

21 **Synthesis of *tert*-butyl 4-[(1-hydroxy-2-naphthoyl)amino]piperidine-1-carboxylate (52):**

22
23
24 To a solution of 91 mg of compound 1-Boc-4-aminopiperidine (0.45 mmol) in 2.5 mL of THF
25
26 was added 86 mg of 1-hydroxy-2-naphtoic acid (1 equiv., 0.45 mmol) and 103 mg of EDCI (1
27
28 equiv., 0.45 mmol). The solution was stirred at reflux for 12 hours. After cooling to room
29
30 temperature, the solution was evaporated to dryness. The crude product was dissolved in 20
31
32 mL of ethyl acetate and the solution was washed with 1N hydrochloric acid solution (3x20mL)
33
34 and then by 10% aqueous sodium carbonate solution. The organic layer was dried over
35
36 Na_2SO_4 , filtered and the solvent is evaporated *in vacuo*. The resulting crude mixture was
37
38 purified by chromatography on silica gel, eluted by *n*Hex/AcOEt 3/1 v/v, to offer compound
39
40 **52** as a white solid (m= 38 mg, 23% yield); ^1H NMR (CDCl_3 , 400 MHz): δ ppm 1.23 (m, 1H), 1.42
41
42 (m, 1H), 1.46 (s, 9H), 2.04 (m, 2H), 2.90 (t, 2H, $J = 12.1$ Hz), 4.07-4.19 (m, 3H), 6.25 (d, 1H, $J =$
43
44 7.7 Hz), 7.23 (d, 1H, $J = 8.8$ Hz), 7.28 (d, 1H, $J = 8.9$ Hz), 7.50 (td, 1H, $J = 8.2$ Hz, 1.3 Hz), 7.56
45
46 (td, 1H, $J = 8.2$ Hz, 1.3 Hz), 7.74 (d, 1H, $J = 7.8$ Hz), 8.40 (d, 1H, $J = 8.2$ Hz), 13.75 (s, 1H); ^{13}C
47
48 NMR (CDCl_3 , 100 MHz): δ ppm 28.6, 29.8, 32.2, 47.3, 80.0, 106.6, 118.3, 120.9, 124.0, 125.8,
49
50 126.0, 127.4, 129.1, 136.4, 154.8, 160.9, 170.2; HPLC, RT= 2.16 min; MS (ESI+): m/z 371.2
51
52 $[\text{M}+\text{H}]^+$, 315.2 $[\text{M}+\text{H}-\text{tBu}]^+$.
53
54
55
56
57
58
59
60

1
2
3 **General procedure for the synthesis of compounds 28-51 and 53.**
4
5

6
7 0.2 mmol of compound **3-25**, **27** or **52** in 5 mL of 6N HCl in dioxane was stirred a room
8
9 temperature for 1h30. The dioxane was evaporated and the crude product was washed with
10
11 diethyl ether to offer deprotected compound as a hydrochloride salt.
12

13
14
15 *N*-(4-(aminomethyl)phenyl)-5-*tert*-butyl-2-hydroxybenzamide hydrochloride (**28**). White solid
16
17 (m= 54 mg, 80% yield); mp: 268-269°C; ¹H NMR (DMSO *d*₆, 300 MHz): δ ppm 1.30 (s, 9H), 3.56
18
19 (s, 1H), 3.99 (s, 2H), 6.97 (d, 1H, *J* = 8.2 Hz), 7.50 (m, 3H), 7.72 (d, 2H, *J* = 7.0 Hz), 7.94 (s, 1H),
20
21 8.42 (bs, 3H), 10.52 (s, 1H); ¹³C NMR (DMSO *d*₆, 75 MHz): δ ppm 31.2, 41.8, 66.3, 116.7, 116.9,
22
23 120.9, 122.8, 125.5, 129.4, 130.6, 138.3, 141.3, 155.7, 166.3; HPLC, RT= 1.45 min; HRMS calcd
24
25 for C₁₈H₂₃N₂O₂ 299.1754, found 299.1752.
26
27
28

29
30
31 2-(4-(aminomethylphenyl)aminomethyl)-4-*tert*-butylphenol hydrochloride (**29**). White solid
32
33 (m= 52 mg, 73% yield); mp: 258-260°C (dec.); ¹H NMR (DMSO *d*₆, 300 MHz): δ ppm 1.20 (s,
34
35 9H), 3.93 (d, 2H, *J* = 5.2 Hz), 4.31 (bs, 2H), 6.81 (d, 1H, *J* = 8.4 Hz), 7.15 (m, 3H), 7.42 (m, 3H),
36
37 8.45 (bs, 3H), 10.43 (s, 1H); ¹³C NMR (DMSO *d*₆, 75 MHz): δ ppm 31.4, 33.7, 41.7, 46.3, 114.7,
38
39 119.0, 120.0, 123.2, 125.8, 127.5, 130.0, 130.3, 140.9, 153.3; HPLC, RT= 1.39 min; HRMS calcd
40
41 for C₁₈H₂₅N₂O 285.1961, found 285.1954.
42
43
44

45
46
47 *N*-(4-(aminomethyl)phenyl)-2-hydroxybenzamide hydrochloride (**30**). White solid (m= 45 mg,
48
49 81% yield); mp: 275-276°C (dec.); ¹H NMR (DMSO *d*₆, 300 MHz): δ ppm 3.99 (d, 2H, *J* = 4.9 Hz),
50
51 6.96 (t, 1H, *J* = 7.5 Hz), 7.04 (d, 1H, *J* = 8.4 Hz), 7.43 (dd, 1H, *J* = 8.4 Hz, 7.2 Hz), 7.49 (d, 2H, *J* =
52
53 8.4 Hz), 7.75 (d, 2H, *J* = 8.4 Hz), 8.01 (d, 1H, *J* = 7.2 Hz), 8.45 (bs, 3H), 10.51 (s, 1H); ¹³C NMR
54
55 (DMSO *d*₆, 75 MHz): δ ppm 41.7, 117.2, 117.5, 119.0, 120.8, 129.2, 129.4, 129.5, 133.6, 138.3,
56
57
58
59
60

1
2
3 158.2, 166.4; HPLC, RT= 1.05 min; MS (ESI+): m/z 244.1 [M+H+1]⁺; HRMS calcd for C₁₄H₁₅N₂O₂
4
5 243.1128, found 243.1129.
6
7

8
9 *N*-(4-(aminomethyl)phenyl)-3-methyl-2-hydroxybenzamide hydrochloride (**31**). Beige solid
10
11 (m= 54 mg, 92% yield); mp: 275-276°C; ¹H NMR (DMSO *d*₆, 400 MHz): δ ppm 2.20 (s, 3H), 4.00
12
13 (q, 2H, *J* = 5.6 Hz), 6.88 (t, 1H, *J* = 7.7 Hz), 7.38 (d, 1H, *J* = 7.7 Hz), 7.51 (d, 2H, *J* = 8.4 Hz), 7.75
14
15 (d, 2H, *J* = 8.4 Hz), 8.00 (d, 1H, *J* = 7.7 Hz), 8.45 (bs, 3H), 10.59 (s, 1H), 12.53 (s, 1H); ¹³C NMR
16
17 (DMSO *d*₆, 100 MHz): δ ppm 15.5, 41.7, 114.1, 118.0, 121.9, 125.5, 126.1, 129.4, 130.1, 135.1,
18
19 137.8, 159.2, 169.2; HPLC, RT= 1.22 min; HRMS calcd for C₁₅H₁₇N₂O₂ 257.1285, found
20
21 257.1292.
22
23
24
25

26
27 *N*-(4-(aminomethyl)phenyl)-4-methyl-2-hydroxybenzamide hydrochloride (**32**). Beige solid
28
29 (m= 53 mg, 90% yield); mp: 282-283°C (dec.); ¹H NMR (DMSO *d*₆, 400 MHz): δ ppm 2.30 (s,
30
31 3H), 3.98 (q, 2H, *J* = 5.6 Hz), 6.78 (d, 1H, *J* = 8.2 Hz), 6.84 (s, 1H), 7.48 (d, 2H, *J* = 8.4 Hz), 7.74
32
33 (d, 2H, *J* = 8.4 Hz), 7.94 (d, 1H, *J* = 8.2 Hz), 8.43 (bs, 3H), 10.46 (s, 1H); ¹³C NMR (DMSO *d*₆, 100
34
35 MHz): δ ppm 21.1, 41.8, 114.2, 117.5, 120.1, 120.9, 129.0, 129.5, 130.3, 138.3, 144.4, 158.8,
36
37 166.7; HPLC, RT= 1.11 min; HRMS calcd for C₁₅H₁₇N₂O₂ 257.1285, found 257.1293.
38
39
40
41

42
43 2 *N*-(4-(aminomethyl)phenyl)-5-methyl-2-hydroxybenzamide hydrochloride (**33**). White solid
44
45 (m= 58 mg, 99% yield); mp: 292-293°C (dec.); ¹H NMR (DMSO *d*₆, 400 MHz): δ ppm 2.28 (s, 3H),
46
47 3.98 (q, 2H, *J* = 5.4 Hz), 6.92 (d, 1H, *J* = 8.3 Hz), 7.24 (d, 1H, *J* = 8.3 Hz), 7.48 (d, 2H, *J* = 8.4 Hz),
48
49 7.74 (d, 2H, *J* = 8.4 Hz), 7.82 (s, 1H), 8.42 (bs, 3H), 10.49 (s, 1H), 11.61 (s, 1H); ¹³C NMR (DMSO
50
51 *d*₆, 100 MHz): δ ppm 20.0, 41.8, 117.1, 120.7, 127.7, 129.1, 129.5, 130.2, 134.3, 138.4, 156.1,
52
53 166.5; HPLC, RT= 1.13 min; HRMS calcd for C₁₅H₁₇N₂O₂ 257.1285, found 257.1289.
54
55
56
57
58
59
60

1
2
3 N-(4-(aminomethyl)phenyl)-6-methyl-2-hydroxybenzamide hydrochloride (**34**). White solid
4
5 (m = 58 mg, 99% yield); mp: 251-252°C (dec.); ¹H NMR (CD₃OD, 300 MHz): δ ppm 2.32 (s, 3H),
6
7 4.10 (s, 2H), 6.72 (d, 1H, *J* = 8.0 Hz), 6.74 (d, 1H, *J* = 8.0 Hz), 7.13 (t, 1H, *J* = 8.0 Hz), 7.44 (d, 2H,
8
9 *J* = 8.5 Hz), 7.78 (d, 2H, *J* = 8.5 Hz); ¹³C NMR (DMSO *d*₆, 100 MHz): δ ppm 19.2, 44.0, 114.0,
10
11 121.7, 122.1, 126.6, 129.9, 130.6, 131.1, 137.5, 141.0, 155.5, 170.1; HPLC, RT = 0.88 min; HRMS
12
13 calcd for C₁₅H₁₇N₂O₂ 257.1285, found 257.1287.
14
15
16
17
18

19 N-(4-(aminomethyl)phenyl)-5-bromo-2-hydroxybenzamide hydrochloride (**35**). Yellow solid
20
21 (m = 71 mg, 99% yield); mp: 309-310°C; ¹H NMR (DMSO *d*₆, 400 MHz): δ ppm 4.00 (s, 2H), 7.01
22
23 (d, 1H, *J* = 8.8 Hz), 7.47 (d, 2H, *J* = 8.6 Hz), 7.58 (dd, 1H, *J* = 8.8 Hz, 2.4 Hz), 7.73 (d, 2H, *J* = 8.6
24
25 Hz), 8.07 (d, 1H, *J* = 2.4 Hz), 8.32 (bs, 3H), 10.50 (s, 1H), 11.90 (bs, 1H); ¹³C NMR (CDCl₃, 100
26
27 MHz): δ ppm 41.8, 110.2, 119.5, 120.7, 129.5, 129.7, 131.4, 135.9, 138.2, 157.1, 164.8; HPLC,
28
29 RT = 1.21 min; HRMS calcd for C₁₄H₁₄N₂O₂Br 321.0233, found 321.0236.
30
31
32
33
34

35 N-(4-(aminomethyl)phenyl)-5-methoxy-2-hydroxybenzamide hydrochloride (**36**). White solid
36
37 (m = 55 mg, 90% yield); mp: 277.5-278.5°C; ¹H NMR (DMSO *d*₆, 300 MHz): δ ppm 3.76 (s, 3H),
38
39 4.00 (s, 2H), 6.95 (d, 1H, *J* = 8.8 Hz), 7.06 (dd, 1H, *J* = 8.8 Hz, 2.2 Hz), 7.47 (d, 2H, *J* = 8.1 Hz),
40
41 7.50 (d, 1H, *J* = 2.2 Hz), 7.74 (d, 2H, *J* = 8.1 Hz), 8.22 (bs, 3H), 10.54 (s, 1H); ¹³C NMR (DMSO *d*₆,
42
43 75 MHz): δ ppm 41.8, 55.7, 112.7, 117.5, 118.2, 120.6, 120.8, 129.5, 129.6, 138.3, 151.8, 152.0,
44
45 165.9; HPLC, RT = 1.10 min; HRMS calcd for C₁₅H₁₇N₂O₃ 273.1234, found 273.1240.
46
47
48
49
50

51 N-(4-(aminomethyl)phenyl)-4-isopropyl-2-hydroxybenzamide hydrochloride (**37**). White solid
52
53 (m = 63 mg, 56% yield); mp: 282-283°C; ¹H NMR (DMSO *d*₆, 400 MHz): δ ppm 1.20 (d, 6H, *J* =
54
55 6.8 Hz), 2.87 (hept, 1H, *J* = 6.8 Hz), 3.99 (d, 2H, *J* = 3.9 Hz), 6.87 (m, 2H), 7.48 (d, 2H, *J* = 8.3 Hz),
56
57 7.74 (d, 2H, *J* = 8.3 Hz), 7.95 (d, 1H, *J* = 7.9 Hz), 8.39 (bs, 3H), 10.5 (s, 1H), 11.97 (bs, 1H); ¹³C
58
59
60

1
2
3 NMR (DMSO d_6 , 100 MHz): δ ppm 23.3, 33.3, 41.8, 114.6, 114.7, 117.4, 120.8, 129.0, 129.4,
4
5 138.3, 155.0, 158.8, 166.7; HPLC, RT= 1.33 min; HRMS calcd for $C_{17}H_{21}N_2O_2$ 285.1598, found
6
7 285.1603.
8
9

10
11 *N*-(4-(aminomethyl)phenyl)-4-trifluoromethyl-2-hydroxybenzamide hydrochloride (**38**).

12
13 White solid (m = 67 mg, 96% yield); mp: 270-272°C (dec.); 1H NMR (DMSO d_6 , 400 MHz): δ
14
15 ppm 3.99 (bs, 2H), 7.28 (d, 1H, $J = 7.9$ Hz), 7.39 (s, 1H), 7.48 (d, 2H, $J = 8.1$ Hz), 7.76 (d, 2H, $J =$
16
17 8.1 Hz), 8.03 (d, 1H, $J = 7.9$ Hz), 8.38 (bs, 3H), 10.54 (s, 1H), 11.97 (bs, 1H); ^{19}F (DMSO d_6 , 400
18
19 MHz): -61.77; ^{13}C NMR (DMSO d_6 , 100 MHz): δ ppm 41.8, 113.4, 115.3, 120.3, 122.1, 123.5,
20
21 129.5, 130.7, 132.3, 132.6, 138.4, 157.1, 164.5; HPLC, RT= 1.29 min; MS (ESI+): m/z 312.1
22
23 [M+H] $^+$, 294.1 [M+H-NH $_3$] $^+$; HRMS calcd for $C_{15}H_{14}F_3N_2O_2$ 311.1002, found 311.1005.
24
25
26
27
28
29

30 *N*-(4-(aminomethyl)phenyl)-4-fluoro-2-hydroxybenzamide hydrochloride (**39**). White solid
31
32 (m= 45 mg, 76% yield); mp: 280-281°C; 1H NMR (DMSO d_6 , 400 MHz): δ ppm 3.99 (s, 2H), 6.88-
33
34 6.80 (m, 2H), 7.48 (d, 2H, $J = 8.4$ Hz), 7.74 (d, 2H, $J = 8.4$ Hz), 8.08 (dd, 1H, $J = 8.7$ Hz, $J = 8.7$
35
36 Hz), 8.36 (bs, 3H), 10.47 (s, 1H), 12.36 (bs, 1H); ^{19}F (DMSO d_6 , 400 MHz): -105.70; ^{13}C NMR
37
38 (DMSO d_6 , 100 MHz): δ ppm 41.8, 103.8 (d, $J = 24.2$ Hz), 106.5 (d, $J = 24.2$ Hz), 114.5, 120.9,
39
40 129.4, 129.6, 131.5 (d, $J = 11$ Hz), 138.2, 160.4 (d, $J = 13.2$ Hz), 164.8 (d, $J = 249$ Hz), 165.7;
41
42 HPLC, RT= 1.09 min; HRMS calcd for $C_{14}H_{14}FN_2O_2$ 261.1034, found 261.1034.
43
44
45
46
47

48 *N*-(4-(aminomethyl)phenyl)-1-hydroxy-2-naphtamide hydrochloride (**40**). White solid (m= 63
49
50 mg, 99% yield); mp: 277-278°C (dec.); 1H NMR (DMSO d_6 , 300 MHz): δ ppm 4.02 (s, 2H), 7.46
51
52 (d, 1H, $J = 8.9$ Hz), 7.53 (d, 2H, $J = 8.3$ Hz), 7.59 (d, 1H, $J = 7.5$ Hz), 7.68 (t, 1H, $J = 7.5$ Hz), 7.80
53
54 (d, 2H, $J = 8.3$ Hz), 7.92 (d, 1H, $J = 8.0$ Hz), 8.22 (d, 1H, $J = 8.9$ Hz), 8.31 (d, 1H, $J = 8.3$ Hz), 8.48
55
56 (bs, 3H), 10.43 (s, 1H); ^{13}C NMR (DMSO d_6 , 75 MHz): δ ppm 41.8, 107.5, 117.8, 122.1, 123.1,
57
58
59
60

1
2
3 123.2, 124.6, 125.9, 127.5, 129.2, 129.4, 130.2, 136.0, 137.8, 160.0, 169.6; HPLC, RT= 1.45 min;
4
5 MS (ESI+): m/z 294.1 [M+H+1]⁺; HRMS calcd for C₁₈H₁₇N₂O₂ 293.1290, found 293.1289.
6
7

8
9 *N*-(4-(aminomethyl)phenyl)-2-hydroxy-1-naphtamide hydrochloride (**41**). White powder (m=
10 57 mg, 97% yield); mp: 248-249°C; ¹H NMR (DMSO *d*₆, 300 MHz): δ ppm 3.98 (d, 2H, *J* = 5.3
11 Hz), 7.32 (m, 2H), 7.45 (m, 3H), 7.67 (d, 1H, *J* = 8.3 Hz), 7.84 (m, 4H), 8.42 (bs, 3H), 10.22 (bs,
12 1H), 10.43 (s, 1H); ¹³C NMR (DMSO *d*₆, 75 MHz): δ ppm 41.9, 118.4, 119.1, 122.9, 123.2, 126.9,
13 127.3, 127.9, 128.6, 129.5, 130.1, 131.3, 139.7, 151.7, 165.8; HPLC, RT= 1.11 min; MS (ESI+):
14 127.3, 127.9, 128.6, 129.5, 130.1, 131.3, 139.7, 151.7, 165.8; HPLC, RT= 1.11 min; MS (ESI+):
15 m/z 294.1 [M+H+1]⁺; HRMS calcd for C₁₈H₁₇N₂O₂ 293.1285, found 293.1293.
16
17
18
19
20
21
22
23

24
25 *N*-(4-(aminomethyl)phenyl)-3-hydroxy-2-naphtamide hydrochloride (**42**). White powder (m=
26 40 mg, 61% yield); mp: 299-300°C (dec.); ¹H NMR (DMSO *d*₆, 400 MHz): δ ppm 4.00 (s, 2H),
27 7.37 (m, 2H), 7.51 (m, 3H), 7.76 (d, 1H, *J* = 8.3 Hz), 7.80 (d, 2H, *J* = 8.4 Hz), 7.94 (d, 1H, *J* = 8.3
28 Hz), 8.35 (bs, 3H), 8.53 (s, 1H), 10.70 (s, 1H), 11.39 (bs, 1H); ¹³C NMR (DMSO *d*₆, 100 MHz): δ
29 ppm 41.8, 110.6, 120.4, 121.8, 123.7, 125.8, 126.9, 128.1, 128.7, 129.4, 129.6, 130.6, 135.8,
30 138.7, 153.6, 165.6; HPLC, RT= 1.26 min; HRMS calcd for C₁₈H₁₇N₂O₂ 293.1285, found
31 293.1286.
32
33
34
35
36
37
38
39
40
41

42
43 *N*-(4-(aminomethyl)phenyl)-2-naphtamide hydrochloride (**43**). White powder (m= 26 mg, 61%
44 yield); mp: 285-286°C (dec.); ¹H NMR (DMSO *d*₆, 500 MHz): δ ppm 4.00 (q, 2H, *J* = 6.0 Hz), 7.50
45 (d, 2H, *J* = 8.5 Hz), 7.64 (m, 2H), 7.88 (d, 2H, *J* = 8.5 Hz), 8.01 (dd, 1H, *J* = 7.6 Hz, 1.4 Hz), 8.05
46 (m, 2H), 8.10 (dd, 1H, *J* = 7.3 Hz, 1.3 Hz), 8.47 (bs, 3H), 8.64 (s, 1H), 10.63 (s, 1H); ¹³C NMR
47 (DMSO *d*₆, 125 MHz): δ ppm 41.9, 120.3, 124.5, 126.9, 127.7, 128.0, 128.1, 128.2, 129.0, 129.2,
48 129.5, 132.0, 132.1, 134.3, 139.4, 165.7; HPLC, RT= 1.21 min; HRMS calcd for C₁₈H₁₇N₂O₂
49 277.1335, found 277.1326.
50
51
52
53
54
55
56
57
58
59
60

1
2
3 *N*-[4-(aminomethyl)phenyl]-1*H*-indole-2-carboxamide (**44**). White solid (m= 40 mg, 76%
4
5 yield); mp: 291-292°C (dec.); ¹H NMR (DMSO *d*₆, 300 MHz): δ ppm 3.98 (q, 2H, *J* = 5.7 Hz), 7.07
6
7 (t, 1H, *J* = 7.8 Hz), 7.22 (t, 1H, *J* = 7.8 Hz), 7.47 (m, 4H), 7.67 (d, 1H, *J* = 8.0 Hz), 7.87 (d, 2H, *J* =
8
9 8.6 Hz), 8.40 (bs, 3H), 10.47 (s, 1H), 11.88 (s, 1H); ¹³C NMR (DMSO *d*₆, 100 MHz): δ ppm 41.9,
10
11 104.4, 112.4, 119.9, 120.0, 121.8, 123.9, 127.0, 128.9, 129.5, 131.4, 136.8, 139.2, 159.7; HPLC,
12
13 RT= 1.82 min; HRMS calcd for C₁₆H₁₆N₃O 266.1288, found 266.1284.
14
15
16
17
18

19 *N*-[4-(aminomethyl)phenyl]-4-oxo-1,4-dihydroquinoline-3-carboxamide (**45**). White solid (m=
20
21 65 mg, 99% yield); mp: 287-289°C (dec.); ¹H NMR (DMSO *d*₆, 400 MHz): δ ppm 3.96 (q, 2H, *J* =
22
23 5.5 Hz), 7.50 (d, 2H, *J* = 8.4 Hz), 7.53 (td, 1H, *J* = 7.9 Hz, 1.3 Hz), 7.76 (d, 2H, *J* = 8.4 Hz), 7.79-
24
25 7.86 (m, 2H), 8.31 (d, 1H, *J* = 7.9 Hz), 8.53 (bs, 3H), 8.82 (d, 1H, *J* = 6.7 Hz), 12.56 (s, 1H), 13.62
26
27 (d, 1H, *J* = 6.4 Hz); ¹³C NMR (DMSO *d*₆, 100 MHz): δ ppm 41.8, 110.3, 119.2, 119.5, 125.3, 125.4,
28
29 125.9, 128.9, 129.9, 133.0, 138.9, 139.1, 143.9, 163.0, 176.3; HPLC, RT= 1.04 min; HRMS calcd
30
31 for C₁₇H₁₆N₃O₂ 294.1237, found 294.1247.
32
33
34
35
36

37 *N*-(4-(aminomethyl)phenyl)-3-hydroxypyridine-2-carboxamide hydrochloride (**46**). Beige solid
38
39 (m= 28 mg, 44% yield); mp: 251-252°C; ¹H NMR (DMSO *d*₆, 300 MHz): δ ppm 4.00 (q, 2H, *J* =
40
41 5.4 Hz), 4.78 (bs, 3H), 7.50 (m, 3H), 7.61 (dd, 1H, *J* = 8.5 Hz, 4.3 Hz), 7.87 (d, 2H, *J* = 8.6 Hz),
42
43 8.27 (dd, 1H, *J* = 4.3 Hz, 1.1 Hz), 8.35 (bs, 2H), 10.99 (s, 1H); ¹³C NMR (DMSO *d*₆, 75 MHz): δ
44
45 ppm 41.8, 121.3, 126.5, 129.4, 129.6, 130.2, 131.2, 137.3, 139.8, 157.6, 167.3; HPLC, RT= 0.95
46
47 min; HRMS calcd for C₁₃H₁₄N₃O₂ 244.1081, found 244.1102.
48
49
50
51
52

53 *N*-(4-(aminomethyl)phenyl)-6-methoxy-1-hydroxy-2-naphthamide hydrochloride (**47**). Beige
54
55 solid (m= 65 mg, 91% yield); mp: 256-257°C (dec.); ¹H NMR (DMSO *d*₆, 300 MHz): δ ppm 3.91
56
57 (s, 3H), 4.02 (s, 2H), 7.19 (dd, 1H, *J* = 9.2, 2.5 Hz), 7.35 (m, 2H), 7.51 (d, 2H, *J* = 8.6 Hz), 7.77 (d,
58
59
60

1
2
3 2H, $J = 8.6$ Hz), 8.14 (d, 1H, $J = 9.2$ Hz), 8.20 (d, 1H, $J = 9.2$ Hz), 8.36 (bs, 3H), 10.55 (bs, 1H),
4
5 14.00 (s, 1H); ^{13}C NMR (DMSO d_6 , 75 MHz): δ ppm 41.8, 55.4, 105.7, 106.4, 117.0, 117.9, 119.4,
6
7 122.0, 123.9, 125.0, 129.4, 130.1, 137.9, 138.1, 159.9, 160.3, 169.7; HPLC, RT= 1.36 min; HRMS
8
9 calcd for $\text{C}_{19}\text{H}_{19}\text{N}_2\text{O}_3$ 323.1390, found 323.1397.
10
11
12

13
14 *N*-(4-(aminomethyl)phenyl)-7-methoxy-1-hydroxy-2-naphtamide hydrochloride (**48**). White
15
16 solid (m= 55 mg, 77% yield); mp: 250-251°C; ^1H NMR (DMSO d_6 , 400 MHz): δ ppm 3.91 (s, 3H),
17
18 4.02 (q, 2H, $J = 5.0$ Hz), 7.32 (dd, 1H, $J = 8.9$ Hz, 2.6 Hz), 7.42 (d, 1H, $J = 8.8$ Hz), 7.51 (d, 2H, $J =$
19
20 8.6 Hz), 7.60 (d, 1H, $J = 2.6$ Hz), 7.79 (d, 2H, $J = 8.6$ Hz), 7.85 (d, 1H, $J = 8.9$ Hz), 8.02 (d, 1H, $J =$
21
22 8.9 Hz), 8.36 (bs, 3H), 10.59 (s, 1H), 13.86 (s, 1H); ^{13}C NMR (DMSO d_6 , 100 MHz): δ ppm 41.8,
23
24 55.2, 101.5, 107.9, 117.7, 120.6, 121.2, 122.1, 125.6, 129.2, 129.4, 130.1, 131.3, 137.8, 157.4,
25
26 158.8, 169.7; HPLC, RT= 1.37 min; HRMS calcd for $\text{C}_{19}\text{H}_{19}\text{N}_2\text{O}_3$ 323.1390, found 323.1403.
27
28
29
30

31
32 *N*-(4-(aminomethyl)phenyl)-7-methyl-1-hydroxy-2-naphtamide hydrochloride (**49**). White
33
34 solid (m= 53 mg, 77% yield); mp: 276-278°C (dec.); ^1H NMR (DMSO d_6 , 500 MHz): δ ppm 3.34
35
36 (s, 3H), 4.01 (s, 2H), 7.40 (d, 1H, $J = 8.7$ Hz), 7.51 (m, 3H), 7.80 (m, 3H), 8.08 (s, 1H), 8.12 (d,
37
38 1H, $J = 8.7$ Hz), 8.44 (bs, 3H), 10.62 (s, 1H), 13.94 (s, 1H); ^{13}C NMR (DMSO d_6 , 125 MHz): δ ppm
39
40 21.4, 41.8, 107.5, 117.6, 122.0, 122.1, 122.2, 124.7, 127.4, 129.4, 130.2, 131.2, 134.2, 135.4,
41
42 137.8, 159.6, 169.7; HPLC, RT= 1.43 min; HRMS calcd for $\text{C}_{19}\text{H}_{19}\text{N}_2\text{O}_2$ 307.1441, found
43
44 307.1452.
45
46
47
48
49

50
51 *N*-(4-(aminomethyl)phenyl)-7-chloro-1-hydroxy-2-naphtamide hydrochloride (**50**). White
52
53 solid (m= 55 mg, 76%); mp: 277-278°C; ^1H NMR (DMSO d_6 , 500 MHz): δ ppm 4.02 (q, 2H, $J =$
54
55 5.6 Hz), 7.53 (m, 3H), 7.70 (dd, 1H, $J = 8.8$ Hz, 2.2 Hz), 7.79 (d, 2H, $J = 8.6$ Hz), 7.99 (d, 1H, $J =$
56
57 8.8 Hz), 8.24 (m, 2H), 8.39 (bs, 3H), 10.73 (s, 1H); ^{13}C NMR (DMSO d_6 , 100 MHz): δ ppm 108.7,
58
59
60

1
2
3 117.8, 121.8, 122.2, 123.8, 125.4, 129.5, 129.6, 129.9, 130.4, 130.8, 134.4, 137.7, 158.8, 169.3;
4
5 HPLC, RT= 1.49 min; HRMS calcd for C₁₈H₁₆N₂O₂Cl 327.0895, found 327.0890.
6
7

8
9 *N*-(4-(aminomethyl)phenyl)-6,7-dimethoxy-1-hydroxy-2-naphthamide hydrochloride **(51)**.

10
11 White solid (m = 62 mg, 80%); mp: 289-291°C (dec.); ¹H NMR (DMSO *d*₆, 400 MHz): δ ppm
12
13 3.90 (s, 3H), 3.92 (s, 3H), 4.01 (q, 2H, *J* = 6.0 Hz), 7.31 (d, 1H, *J* = 8.8 Hz), 7.33 (s, 1H), 7.51 (d,
14
15 2H, *J* = 8.6 Hz), 7.55 (s, 1H), 7.79 (d, 2H, *J* = 8.6 Hz), 8.03 (d, 1H, *J* = 8.8 Hz), 8.45 (bs, 3H),
16
17 10.53 (s, 1H), 13.85 (s, 1H); ¹³C NMR (DMSO *d*₆, 100 MHz): δ ppm 55.4, 55.6, 66.3, 101.8,
18
19 106.1, 106.7, 116.6, 119.2, 121.4, 121.9, 129.4, 130.0, 132.5, 137.9, 149.0, 151.6, 158.8,
20
21 169.8; HPLC, RT= 2.28 min; HRMS calcd for C₂₀H₂₁N₂O₄ 353.1496, found 353.1496.
22
23
24
25

26
27 1-Hydroxy-*N*-piperidin-4-yl-2-naphthamide **(53)**. White solid (m = 43 mg, 70% yield); mp:
28
29 279-280°C; ¹H NMR (DMSO *d*₆, 400 MHz): δ ppm 1.89-2.02 (m, 4H), 3.02 (m, 2H), 3.33 (d, 2H,
30
31 *J* = 12.8 Hz), 4.19 (m, 1H), 7.37 (d, 1H, *J* = 8.8 Hz), 7.55 (td, 1H, *J* = 8.1 Hz, 1.1 Hz), 7.63 (td, 1H,
32
33 *J* = 8.1 Hz, 1.2 Hz), 7.87 (d, 1H, *J* = 8.1 Hz), 8.03 (d, 1H, *J* = 8.8 Hz), 8.25 (d, 1H, *J* = 8.1 Hz), 8.98
34
35 (d, 1H, *J* = 8.1 Hz), 9.08 (bs, 2H), 14.50 (s, 1H); ¹³C NMR (DMSO *d*₆, 100 MHz): δ ppm 27.9,
36
37 44.5, 66.3, 106.9, 117.4, 122.9, 123.0, 124.6, 125.7, 127.4, 128.9, 135.8, 159.7, 170.1; HPLC,
38
39 RT= 1.28 min; HRMS calcd for C₁₆H₁₉N₂O₂ 271.1441, found 271.1439.
40
41
42
43
44
45
46

47 Enzymes and chemicals

48
49 KLK6 was purchased from R&D Systems® as pro-KLK6. Activation of KLK6 is performed in 50
50 mM Tris, 0.05% (w/v) Brij-35, pH 8.0. The activation reaction is initiated by lysyl-
51
52 endopeptidase at 2.5 mU.mL⁻¹ (Wako Bioproducts®). The activation reaction is stopped by
53
54 diluting KLK6 to 0.5 µg.mL⁻¹ in assay buffer (50 mM Tris, 1 M Citrate, 0.05% (w/v) Brij-35, pH
55
56 7.4) to obtain an active KLK6 stock. KLK1 was purchased from R & D Systems® as pro-KLK1.
57
58
59
60

1
2
3 Activation of KLK1 is performed in 50 mM Tris-HCl, 10mM CaCl₂, 150 mM NaCl, 0.05% Brij-35,
4
5 pH 7.5. The activation reaction is initiated by bacterial thermolysin at 0.4 µg.mL⁻¹ (Sigma-
6
7 Aldrich®) and stopped by addition of 100 mM EDTA (Sigma-Aldrich®) to obtain an active KLK1
8
9 stock at the same concentration of 100 µg.mL⁻¹. Plasmin (Sigma-Aldrich®) and Caspase-2,
10
11 Caspase-3, Caspase-6 (Enzo Life Sciences®) were purchased in mature and active form. All
12
13 enzyme stocks were stored at -20 ° C. KLK4, KLK5, KLK7, KLK8, KLK11, KLK13; thrombin,
14
15 cathepsin L, matriptase, trypsin, trypsin-3 and tPA were purchased from R&D Systems® as pro-
16
17 enzymes (KLK4, KLK7, KLK8, KLK11, KLK13) or as mature and active forms (KLK5, thrombin,
18
19 cathepsin L, matriptase, trypsin-3, tPA). Activation of KLK4, KLK7, KLK8, KLK11 and KLK13 are
20
21 performed in optimized buffers. The activation reactions for KLK4, KLK7 and KLK11 are
22
23 initiated bacterial thermolysin at 0.4 µg.mL⁻¹ (Sigma-Aldrich®) and stopped by addition of 100
24
25 mM EDTA (Sigma-Aldrich®) to obtain active stocks. All enzyme stocks were stored at -20°C. H-
26
27 PFR-AMC (KLK1), Boc-VPR-AMC (KLK4, KLK5, KLK8, KLK13, KLK14, Thrombin), Boc-QAR-AMC
28
29 (KLK6, KLK11, Matriptase, Trypsin, Trypsin-3, Plasmin), Ac-VDVAD-AMC (Caspase-2), Ac-DEVD-
30
31 AMC (Caspase-3), Ac-VEID-AMC (Caspase-6), Z-LR-AMC (Cathepsin L), Z-GGR-AMC (tPA)
32
33 substrates were purchased from Bachem®. MeO-Suc-RPY-AMC (KLK7) substrate was
34
35 purchased from AAT Bioquest®.

46 47 **Kinetics assays**

48
49 Compounds were screened on KLK6, KLK1 and plasmin using a using a BMG Fluostar
50
51 microplate reader (black 96-well microplates). The proteases are preincubated for 15 minutes
52
53 with each compound (10 µM and 50 µM) or with DMSO (<2%, negative control) in a total
54
55 volume of 100 µl of 50 mM Tris buffer, 1 M citrate, 0.05% Brij-35, pH 7, 37 ° C. The reaction is
56
57 triggered by adding the Boc-QAR-AMC (KLK6, plasmin) or H-PFR-AMC (KLK1) fluorogenic
58
59
60

1
2
3 substrate (100 μM) and followed for 30 minutes at 37°C. The release of the AMC fluorescent
4
5 group is detected using the following wavelengths: $\lambda_{\text{ex}} = 360 \text{ nm}$ for the excitation and $\lambda_{\text{em}} =$
6
7 460 nm for the measurement of the emission. The percent inhibition is calculated from
8
9 equation 1 where V_0 is the initial rate of the DMSO control, the initial rate in the presence of
10
11 the inhibitor V_i .
12
13

$$\% \text{ Inhibition} = (1 - (V_i / V_0)) * 100 \text{ (Eq. 1)}$$

14
15
16
17 The selected compounds are those for which the inhibition is greater than 50% at a
18
19 concentration of 10 μM then the IC_{50} is determined. The inhibitory effect of the compound
20
21 (%) as a function of its concentration generally follows the Eq. 2 which results in a
22
23 hyperbole or a sigmoid. The equation is entered in the Kaleidagraph® 4.5 software for curve
24
25 fitting $f([I]) = \% \text{ Inhibition}$, where $[I]$ is the inhibitor concentration. The concentration ranges
26
27 of inhibitor were adjusted to inhibitory potency as detected in preliminary screening tests,
28
29 $[I]$ was from 0.1 μM to 100 μM .
30
31
32
33

34
35 The inhibitory activity of compounds was expressed as IC_{50} (inhibitor concentrations giving
36
37 50% inhibition). The values of IC_{50} were calculated by fitting the experimental data to the
38
39 Equation 2a and 2b:
40
41

$$\% \text{ Inhibition} = 100 \times (1 - V_i / V_0) = 100 [I]_0 / (\text{IC}_{50} + [I]_0), \text{ (Eq 2a)}$$

$$\% \text{ Inhibition} = 100 [I]_0^{n_H} / (\text{IC}_{50}^{n_H} + [I]_0^{n_H}), \text{ where } n_H \text{ is the Hill number. (Eq 2b)}$$

42
43
44
45 Reversibility was analysed by diluting the reaction mixtures (dilution factor of 100) after 15
46
47 and 60 min preincubation of the enzyme with inhibitor. Aliquots of reaction mixtures (2.5
48
49 μL) were added to 97.5 μL of buffer containing the fluorogenic substrate (experimental
50
51 conditions identical to the routine protocol used for a given enzyme). The mechanism of
52
53 inhibition was determined by varying substrate and inhibitor concentrations, the type of
54
55 inhibition and inhibition parameter (K_i) are determined by Dixon's plots.
56
57
58
59
60

Selectivity profiling

Hit compounds were screened on the selected group of CNS proteases using optimized concentrations and buffers (KLK4 9.6 nM; KLK5 0.85 nM; KLK7 19 nM; KLK8 0.88 nM; KLK11 67 nM; KLK13 0.2 nM; KLK14 0.6 nM; Caspase-2 0.2 nM; Caspase-3 0.1 nM; Caspase-6 68.5 mU. μL^{-1} ; Cathepsin L 0.12 nM; Matriptase 0.69 nM; Thrombin 25 pM; tPA 6.7 nM; Trypsin 0.63 pM ;Trypsin-3 0.8 pM ;Plasmin 3 nM). The reaction is triggered by the appropriate substrate at the optimized concentration (H-PFR-AMC 100 μM ; Boc-VPR-AMC 100 μM ; Boc-QAR-AMC 100 μM ; Meo-Suc-RPY-AMC 100 μM ; Ac-VDVAD-AMC 25 μM ; Ac-DEVD-AMC 10 μM ; Ac-VEID-AMC 100 μM ; Z-LR-AMC 50 μM ; Z-GGR-AMC 100 μM) and followed for 30 minutes at 37°C. Percentages of inhibition at 10 μM of each compound are determined as described in previous paragraph. Results are given from 3 independent experiments with a standard error below 10%.

Molecular docking

Molecular docking experiments were conducted to propose interaction models of the hit *para*-aminobenzyl derivatives **32** and **42** with KLK6. The protonation states of the ligands were calculated using MarvinSketch[®] at pH = 7. The major microspecy described the primary amine function charged, while the rest of the molecules was neutral (protonated alcohol function). The 3D conformations of both ligands were generated by MarvinSketch[®]. The structure of the target was retrieved from the Protein Data Bank, and chose due to the presence of an orthosteric inhibitor similar in structure to the *para*-aminobenzyl derivatives in order to shape the binding pocket to these two compounds (PDB id: 4D8N^{33,45}). The protonation state of the target was predicted with Propka.⁴⁶ The catalytic histidine was found charged and protonated

1
2
3 on both nitrogens, while other residues and termini were found in their canonical state at pH
4
5 7. The ligands and target were prepared using Autodock Tools 4⁴⁷ before flexible molecular
6
7 docking with Autodock Vina.⁴⁸ Q192 and S195 side chains were found in different orientations
8
9 in other KLK6 structures. These two residues were set flexible in the molecular docking routine
10
11 in order to increase the reliability of the results. Including this protein flexibility, the number
12
13 of degrees of freedom (dof) was still in an acceptable range for Vina (10 dof, while Vina is
14
15 designed to converge properly until 12 dof). The box was centered near the geometrical
16
17 center of the S1 binding pocket (residue: H57, D189 to S195, S214 to N217, C220), with a final
18
19 size of 18x19x18 Å³ which largely included S1, S1', S2 and S2'. 20 poses were asked with an
20
21 exhaustiveness of 128. The poses were then re-scored using Convex-PL⁴⁹ and the best poses
22
23 according to this new scoring function of both compounds into KLK6 were further analyzed.
24
25 The coordinate files of both poses are available in the online version.
26
27
28
29
30
31
32
33
34

35 ***Neuronal cytotoxicity of hit compounds***

36
37 All animals were ethically maintained and used in compliance with the European Policy on
38
39 Ethics. Cortices and striatum were microdissected from E14 embryos of Swiss mice (Janvier,
40
41 Labs Le Genest Saint Isle, France) in D-PBS supplemented with 0.1% (w/w) glucose
42
43 (ThermoFisher Scientific; 15023-021). Dissected structures were digested with trypsin/EDTA
44
45 (ThermoFisher Scientific; R001100) for 15 minutes at room temperature. After trypsin
46
47 inactivation with 10% (v/v) fetal bovine serum (10500056; ThermoFisher Scientific), structures
48
49 were mechanically dissociated with a pipette in Neurobasal media (ThermoFisher Scientific;
50
51 2110349) supplemented with DNase I (ThermoFisher Scientific; EN0525), B27 (ThermoFisher
52
53 Scientific; 17504-044); L-Glutamine (ThermoFisher Scientific; 25030-024),
54
55 Penicillin/Streptomycin (ThermoFisher Scientific, 1540-122). Cortical and striatal cells were
56
57
58
59
60

1
2
3 then seeded at the density of 100 000 cells/well in sterile transparent 96 well plates previously
4 coated. Cells are cultured for 7 days at 37°C in a 5% CO₂ atmosphere. Cells were treated for
5
6 24 hours either with inhibitors at different concentrations (10, 25, 50 or 100 µM) or with the
7
8 vehicle DMSO 1% (negative control, vehicle) or with rotenone 50 µM (positive control). The
9
10 treatment of primary cultures of neurons by rotenone is a standard compound used to induce
11
12 neuronal death. Medium is then replaced with 50 µL of XTT (0.3 mg.mL⁻¹) for 3 hours in order
13
14 to carry out the cell viability test (Merck; 11465015001). XTT is a derivative of tetrazolium salt
15
16 whose reduction by mitochondrial dehydrogenase viable cells shows a yellow-orange
17
18 coloring. The activity of the mitochondria is determined by measuring the absorbance at 485
19
20 nm. The percentage of cell survival is calculated by the ratio of the absorbance in the presence
21
22 of the inhibitor to the negative control condition (DMSO 1%). Statistical analyses of differences
23
24 between treatments were assessed by a Kruskal-Wallis test using GraphPad Prism 7.03. For
25
26 all analysis * p-value < 0.05; ** p-value < 0.01; *** p-value < 0.001.
27
28
29
30
31
32
33

Evaluation of the effect of compounds on oligodendrocyte differentiation

B104 cell culture

34
35
36
37 B104 cells were cultured in flasks (TPP) containing DMEM (Gibco) supplemented with 1%
38
39 penicillin-streptomycin (Gibco), 1% Non-Essential Amino Acids Solution (Gibco) and 10% Fetal
40
41 Bovine Serum (FBS; Gibco) and passaged every week using Trypsin 0.25% (Gibco; 25200056).
42
43 This medium was changed after 4 days for N1 medium w/o biotin. This B104-conditioned
44
45 medium containing growth factors was collected after 3 days and used to prepare N1B104
46
47
48
49
50
51
52
53
54
55
56
57
58
59
60
61
62
63
64
65
66
67
68
69
70
71
72
73
74
75
76
77
78
79
80
81
82
83
84
85
86
87
88
89
90
91
92
93
94
95
96
97
98
99
100
101
102
103
104
105
106
107
108
109
110
111
112
113
114
115
116
117
118
119
120
121
122
123
124
125
126
127
128
129
130
131
132
133
134
135
136
137
138
139
140
141
142
143
144
145
146
147
148
149
150
151
152
153
154
155
156
157
158
159
160
161
162
163
164
165
166
167
168
169
170
171
172
173
174
175
176
177
178
179
180
181
182
183
184
185
186
187
188
189
190
191
192
193
194
195
196
197
198
199
200
201
202
203
204
205
206
207
208
209
210
211
212
213
214
215
216
217
218
219
220
221
222
223
224
225
226
227
228
229
230
231
232
233
234
235
236
237
238
239
240
241
242
243
244
245
246
247
248
249
250
251
252
253
254
255
256
257
258
259
260
261
262
263
264
265
266
267
268
269
270
271
272
273
274
275
276
277
278
279
280
281
282
283
284
285
286
287
288
289
290
291
292
293
294
295
296
297
298
299
300
301
302
303
304
305
306
307
308
309
310
311
312
313
314
315
316
317
318
319
320
321
322
323
324
325
326
327
328
329
330
331
332
333
334
335
336
337
338
339
340
341
342
343
344
345
346
347
348
349
350
351
352
353
354
355
356
357
358
359
360
361
362
363
364
365
366
367
368
369
370
371
372
373
374
375
376
377
378
379
380
381
382
383
384
385
386
387
388
389
390
391
392
393
394
395
396
397
398
399
400
401
402
403
404
405
406
407
408
409
410
411
412
413
414
415
416
417
418
419
420
421
422
423
424
425
426
427
428
429
430
431
432
433
434
435
436
437
438
439
440
441
442
443
444
445
446
447
448
449
450
451
452
453
454
455
456
457
458
459
460
461
462
463
464
465
466
467
468
469
470
471
472
473
474
475
476
477
478
479
480
481
482
483
484
485
486
487
488
489
490
491
492
493
494
495
496
497
498
499
500
501
502
503
504
505
506
507
508
509
510
511
512
513
514
515
516
517
518
519
520
521
522
523
524
525
526
527
528
529
530
531
532
533
534
535
536
537
538
539
540
541
542
543
544
545
546
547
548
549
550
551
552
553
554
555
556
557
558
559
560
561
562
563
564
565
566
567
568
569
570
571
572
573
574
575
576
577
578
579
580
581
582
583
584
585
586
587
588
589
590
591
592
593
594
595
596
597
598
599
600
601
602
603
604
605
606
607
608
609
610
611
612
613
614
615
616
617
618
619
620
621
622
623
624
625
626
627
628
629
630
631
632
633
634
635
636
637
638
639
640
641
642
643
644
645
646
647
648
649
650
651
652
653
654
655
656
657
658
659
660
661
662
663
664
665
666
667
668
669
670
671
672
673
674
675
676
677
678
679
680
681
682
683
684
685
686
687
688
689
690
691
692
693
694
695
696
697
698
699
700
701
702
703
704
705
706
707
708
709
710
711
712
713
714
715
716
717
718
719
720
721
722
723
724
725
726
727
728
729
730
731
732
733
734
735
736
737
738
739
740
741
742
743
744
745
746
747
748
749
750
751
752
753
754
755
756
757
758
759
760
761
762
763
764
765
766
767
768
769
770
771
772
773
774
775
776
777
778
779
780
781
782
783
784
785
786
787
788
789
790
791
792
793
794
795
796
797
798
799
800
801
802
803
804
805
806
807
808
809
810
811
812
813
814
815
816
817
818
819
820
821
822
823
824
825
826
827
828
829
830
831
832
833
834
835
836
837
838
839
840
841
842
843
844
845
846
847
848
849
850
851
852
853
854
855
856
857
858
859
860
861
862
863
864
865
866
867
868
869
870
871
872
873
874
875
876
877
878
879
880
881
882
883
884
885
886
887
888
889
890
891
892
893
894
895
896
897
898
899
900
901
902
903
904
905
906
907
908
909
910
911
912
913
914
915
916
917
918
919
920
921
922
923
924
925
926
927
928
929
930
931
932
933
934
935
936
937
938
939
940
941
942
943
944
945
946
947
948
949
950
951
952
953
954
955
956
957
958
959
960
961
962
963
964
965
966
967
968
969
970
971
972
973
974
975
976
977
978
979
980
981
982
983
984
985
986
987
988
989
990
991
992
993
994
995
996
997
998
999
1000

CG4 cell line culture

CG4 cells were cultured in culture flasks (TPP) coated with 0.01% Poly-L-Ornithine (Sigma) with filtered N1B104 medium to ensure proliferation. Cells were passaged with Trypsin 0.05% (Gibco) when reaching 60-70% confluence.⁵² The CG4 line used in this study expressed the fluorescent reporters GFP at all developmental stages of the oligodendroglial cell lineage and mCherry only in differentiated and mature oligodendrocytes (Deboux *et al.* in preparation). For differentiation assay, CG4 cells were seeded in N1B104 medium in 96 well plates (Nunc) at the density of 6500 cell/cm² for few hours. Cells were then switched in a differentiation medium (DMEM/F12 1:1 (Gibco) supplemented with 2% B27 (Gibco); 1% laminin (Sigma) and 1% N1 biotin) with or without the compounds. The 9-cis-retinoic acid at 1 μ M (Sigma) was as positive control. Cells were differentiated for 5 days before image acquisition and quantification on an Arrayscan XTI System (Thermo Scientific).

Oligodendrocyte precursor cell (OPCs) primary cell cultures

Primary OPCs cultured were derived from Wistar rats' cerebral cortices at P1, as previously described.⁵⁰ Briefly, the cerebral cortices were dissected and the meninges were removed in DME, 1% penicillin-streptomycin and 1% MEM NEAA. Tissues were dissociated enzymatically using trypsin-EDTA solution for 10 min at 37°C. Cell suspension was filtered with 70 μ m nylon cell strainer, centrifuged at 1000 rpm for 10 min and resuspended in an appropriate volume of DMEM/10% FBS for seeding (10 ml per flask/ 2 brains in each) in culture flasks coated with 0.01% poly-L-ornithine and incubated at 5% CO₂ and 37°C for approximately two weeks. The medium was changed at day 7. After 14 DIV, cells were shaken for 2h at 250 rpm to remove microglia⁵¹. An additional shaking is performed overnight at 250 rpm to detach and collect OPCs. Collected OPCs were plated on Poly-Ornithine coated 24-well plates, at a density of 25

1
2
3 000 cells/well. OPCs were kept in proliferation medium containing DMEM/F12 (1:1),
4
5 supplemented with 2% B27 (all purchased from Gibco), FGF and PDGF (10 ng/ml each) to
6
7 allow adhesion. The medium is then changed for a differentiation medium with or
8
9 without the compounds. As for the CG4 cultures, 9-cis-retinoic acid at 1 μ M was used as a
10
11 positive control. Cells were kept in differentiation medium for 5 days, before image
12
13 acquisition and quantification on an Arrayscan XTI System (Thermo Scientific).
14
15
16
17
18
19

20 *Immunostaining*

21
22 Cells were fixed with 2% paraformaldehyde (Electron Microscopy) for 5mn at room
23
24 temperature, washed with PBS 1X and stored at 4°C prior to staining. They were incubated
25
26 for 1 hour at RT in 4% BSA (Sigma); 1X PBS, 0.1% Triton X-100 and primary antibodies. They
27
28 were next rinsed three times with PBS 1X and incubated for 45mn at RT in 4% BSA in 1X PBS, 1
29
30 μ g/ml Hoechst dye (Sigma, B2261) and secondary antibodies. After incubation, plates were
31
32 washed three times with PBS 1X. Image acquisitions and quantification were performed as
33
34 described above.
35
36
37
38

39
40 The line used is a rat oligodendrocyte precursor (CG4) CG4 cell line, stably transduced with
41
42 the GFP reporter gene under the control of the CMV promoter and mCherry under the control
43
44 of a differentiated oligodendrocyte specific promoter. The mCherry marker is only expressed
45
46 at the differentiated oligodendrocyte stage and thus makes it possible to test compounds
47
48 capable of inducing differentiation of OPCs. The cells are cultured in the proliferation
49
50 medium described by Louis et al. ⁵² at the time of their enumeration, then in a
51
52 medium of differentiation (DMEM / F12, B27, N1, biotin, laminin). The cells are treated
53
54 with different inhibitor concentrations for 72 h in 96-well plates and then screened using
55
56 an automated inverted microscope. The experimental controls used are a basal control
57
58 containing only the
59
60

1
2
3 differentiation medium and a positive control, 9-cis-retinoic acid, known for its effect in
4
5 inducing differentiation of OPCs.⁵³ To evaluate the effects of the compounds on OPC
6
7 differentiation, we quantified the number of mCherry+ and GFP+ cells in each experimental
8
9 condition relatively to the basal control. An effect in favor of differentiation is reflected in a
10
11 significant increase in the number of mCherry+ cells, in contrast to an effect to the detriment
12
13 of differentiation. The results are analyzed using the Mann-Whitney statistical test.
14
15
16
17
18
19

20 **Anti-inflammatory potential**

21
22 The impact of compounds on microglial activation and pro-inflammatory cytokines was
23
24 assessed in purified primary microglial cultures isolated from newborn rat brain, as previously
25
26 described.³⁶ All animals used were handled in accordance with European standards for ethics and
27
28 animal welfare. The new born WISTAR rats (Janvier Labs®, Le Genest Saint Isle, France) at stage P1 are
29
30 sacrificed by decapitation. After removal of the meninges, the cortical structures are removed in
31
32 DMEM medium containing 1% of penicillin / streptomycin mix (Thermofisher®, 15070063) and 1% of
33
34 non-essential amino acids (MEM NEAA, Thermofisher®, 11140050). Tissues are enzymatically
35
36 dissociated by the addition of trypsin-EDTA (Gibco®, 25200056) for 10 minutes at 37 ° C. Cell
37
38 suspension is then passed through a nylon filter 70 µm in diameter, centrifuged at 1000 rpm for 10
39
40 minutes then resuspended in a volume of 10 mL of DMEM medium supplemented with 10% FCS
41
42 (Thermofisher Scientific®, 10500056) in a flask previously coated with 0.01% poly-L-ornithine (Sigma-
43
44 Aldrich®, P4957). Cells are cultured for two weeks at 37 ° C in a humid atmosphere (5% CO₂) with a
45
46 change of medium on the seventh day. At the end of this period, the cells are stirred for 2 hours at 250
47
48 rpm to detach and recover the microglia. Cells are inoculated into sterile transparent 96-well FALCON®
49
50 plates at a density of 50,000 cells / well in DMEM / F12 medium supplemented with 1% N2 mix, then
51
52 cultured for 24 hours at 37 ° C in a humid atmosphere (5% CO₂). The microglia is treated with
53
54 lipopolysaccharide (LPS, 10 ng.mL⁻¹, Sigma Aldrich®) to create an inflammatory environment to be
55
56
57
58
59
60

1
2
3 activated. Concomitantly, cells are treated either with inhibitors at different concentrations defined
4
5 according to the IC₅₀ values (0.5 – 10 μM), or with 1% DMSO (negative control), or with 100 nM
6
7 dexamethasone (positive anti-inflammatory control, Sigma -Aldrich® D4902) for 3 hours at 37 ° C in a
8
9 humid atmosphere (5% CO₂). At the end of this incubation, supernatants are recovered for assays of
10
11 pro-inflammatory cytokines TNF-α and IL1-β by ELISA (Rat TNF-α ELISA MAX™ Deluxe Set # 438204,
12
13 rat IL1-β ELISA kit ab100768)
14
15
16
17
18
19
20
21
22
23
24
25
26
27
28
29
30
31
32
33
34
35
36
37
38
39
40
41
42
43
44
45
46
47
48
49
50
51
52
53
54
55
56
57
58
59
60

Associated content

The supporting information is available free of charge on the ACS Publications website.

Supplementary figures: compounds synthesis and characterization data, Dixon plot of compounds **37** and **47** towards KLK6 (**Figure S1**), Structure of synthesized compounds (**Table S1**), comparative table of ADME and pharmacological parameters for hit compounds **32** and **42** (**Table S2**).

Models of compounds **32** and **42** docked on 4D8N KLK6 pdb files. (PDB)

Molecular formula strings of compounds described in this study (CSV)

Author information

Corresponding authors

Email: Chahrazade.el_amri@sorbonne-universite.fr

Address

Sorbonne Université, Faculty of Sciences and Engineering, IBPS, UMR 8256 CNRS-UPMC, ERL INSERM U1164, Biological Adaptation and Ageing, F-75252 Paris, France. Paris, France

Author contributions

The research was designed by CE, NM, BNO. Chemical synthesis was performed by NM. Enzymology assays were performed by SAA, NC and FS, biological with neural cells, OPCs and microglial by SAA and CD. Docking models were determined by ML. ED and SB contributed to experiments on primary cultures of neural cells. Data analysis and manuscript preparation were done by CE, NM and BNO. All the authors have given approval the final version of the manuscript.

Notes

The authors declare no competing financial interest.

Acknowledgements:

The authors are grateful to Sorbonne Université, Université of Montpellier, Institut National pour la Recherche Médicale (INSERM), Centre National de la Recherche Scientifique (CNRS) as well as the SATT Lutech for research funding. The authors wish to thank Dr David Akbar (ICM Cell Culture Facility, CELIS) for his advice and technical assistance on fluorescence imaging and quantitative analysis. This study was supported by the Investissements d’Avenir ANR-10-IAIHU-06 (IHU-A-ICM) and ANR-11-INBS-0011 (NeurATRIS) (to B.N-O.) We also thank the French Ministry of Research and Education for S A and F. S PhD fellowships.

Abbreviations used

ADMET, Absorption Diffusion Metabolism, Elimination and Toxicity; CNS, central nervous system; DMEM, Dulbecco’s modified Eagle’s medium; DMSO, dimethyl sulfoxide; EDCI, N-(3-dimethylaminopropyl)-N'-ethylcarbodiimide hydrochloride; IL1 β : interleukin 1 β ; KLK, tissue kallikreins; KLK1, kallikrein-related peptidase 1; KLK6, kallikrein-related peptidase 6; LPS, lipopolysaccharide; MBP, myelin basic protein; MS, multiple sclerosis; OPC, oligodendrocyte precursor cell; PAR, Protease-Activated receptors; TNF β : tumor necrosis factor.

References

1. Lassmann, H. Multiple Sclerosis Pathology. *Cold Spring Harb Perspect Med* **2018**, 8, 1-15.
2. Friese, M. A.; Schattling, B.; Fugger, L. Mechanisms of neurodegeneration and axonal dysfunction in multiple sclerosis. *Nat Rev Neurol* **2014**, 10, 225-238.
3. Kuhlmann, T.; Miron, V.; Cui, Q.; Wegner, C.; Antel, J.; Bruck, W. Differentiation block of oligodendroglial progenitor cells as a cause for remyelination failure in chronic multiple sclerosis. *Brain* **2008**, 131, 1749-1758.
4. Bove, R. M.; Green, A. J. Remyelinating Pharmacotherapies in Multiple Sclerosis. *Neurotherapeutics* **2017**, 14, 894-904.
5. Cole, K. L. H.; Early, J. J.; Lyons, D. A. Drug discovery for remyelination and treatment of MS. *Glia* **2017**, 65, 1565-1589.
6. Franklin, R. J. M.; Ffrench-Constant, C. Regenerating CNS myelin - from mechanisms to experimental medicines. *Nat Rev Neurosci* **2017**, 18, 753-769.
7. Coetzee, T.; Thompson, A. J. Unified understanding of MS course is required for drug development. *Nat Rev Neurol* **2018**, 14, 191-192.
8. Cunniffe, N.; Coles, A. Promoting remyelination in multiple sclerosis. *J Neurol* **2021**, 268, 30-44.
9. Murakami, K.; Jiang, Y. P.; Tanaka, T.; Bando, Y.; Mitrovic, B.; Yoshida, S. In vivo analysis of kallikrein-related peptidase 6 (KLK6) function in oligodendrocyte development and the expression of myelin proteins. *Neuroscience* **2013**, 236, 1-11.
10. Bando, Y.; Ito, S.; Nagai, Y.; Terayama, R.; Kishibe, M.; Jiang, Y. P.; Mitrovic, B.; Takahashi, T.; Yoshida, S. Implications of protease M/neurosin in myelination during experimental demyelination and remyelination. *Neurosci Lett* **2006**, 405, 175-180.

- 1
2
3 11. Scarisbrick, I. A.; Isackson, P. J.; Ciric, B.; Windebank, A. J.; Rodriguez, M. MSP, a trypsin-
4 like serine protease, is abundantly expressed in the human nervous system. *J Comp Neurol*
5
6 **2001**, 431, 347-361.
7
- 8
9
10 12. Bando, Y.; Hagiwara, Y.; Suzuki, Y.; Yoshida, K.; Aburakawa, Y.; Kimura, T.; Murakami,
11
12 C.; Ono, M.; Tanaka, T.; Jiang, Y. P.; Mitrovi, B.; Bochimoto, H.; Yahara, O.; Yoshida, S. Kallikrein
13
14 6 secreted by oligodendrocytes regulates the progression of experimental autoimmune
15
16 encephalomyelitis. *Glia* **2018**, 66, 359-378.
17
- 18
19
20 13. Burda, J. E.; Radulovic, M.; Yoon, H.; Scarisbrick, I. A. Critical role for PAR1 in kallikrein
21
22 6-mediated oligodendrogliopathy. *Glia* **2013**, 61, 1456-1470.
23
- 24
25 14. Yoon, H.; Radulovic, M.; Scarisbrick, I. A. Kallikrein-related peptidase 6 orchestrates
26
27 astrocyte form and function through proteinase activated receptor-dependent mechanisms.
28
29 *Biol Chem* **2018**, 399, 1041-1052.
30
- 31
32 15. Yoon, H.; Radulovic, M.; Walters, G.; Paulsen, A. R.; Drucker, K.; Starski, P.; Wu, J.;
33
34 Fairlie, D. P.; Scarisbrick, I. A. Protease activated receptor 2 controls myelin development,
35
36 resiliency and repair. *Glia* **2017**, 65, 2070-2086.
37
- 38
39 16. Radulovic, M.; Yoon, H.; Wu, J.; Mustafa, K.; Scarisbrick, I. A. Targeting the thrombin
40
41 receptor modulates inflammation and astrogliosis to improve recovery after spinal cord injury.
42
43 *Neurobiol Dis* **2016**, 93, 226-242.
44
- 45
46 17. Panos, M.; Christophi, G. P.; Rodriguez, M.; Scarisbrick, I. A. Differential expression of
47
48 multiple kallikreins in a viral model of multiple sclerosis points to unique roles in the innate
49
50 and adaptive immune response. *Biol Chem* **2014**, 395, 1063-1073.
51
- 52
53 18. Kroksveen, A. C.; Aasebo, E.; Vethe, H.; Van Pesch, V.; Franciotta, D.; Teunissen, C. E.;
54
55 Ulvik, R. J.; Vedeler, C.; Myhr, K. M.; Barsnes, H.; Berven, F. S. Discovery and initial verification
56
57
58
59
60

1
2
3 of differentially abundant proteins between multiple sclerosis patients and controls using
4 iTRAQ and SID-SRM. *J Proteomics* **2013**, 78, 312-325.

7
8 19. Scarisbrick, I. A. The multiple sclerosis degradome: enzymatic cascades in development
9 and progression of central nervous system inflammatory disease. *Curr Top Microbiol Immunol*
10 **2008**, 318, 133-175.

13
14
15 20. Blaber, S. I.; Ciric, B.; Christophi, G. P.; Bennett, M. J.; Blaber, M.; Rodriguez, M.;
16 Scarisbrick, I. A. Targeting kallikrein 6 proteolysis attenuates CNS inflammatory disease. *FASEB*
17 *J* **2004**, 18, 920-932.

20
21 21. Yoon, H.; Blaber, S. I.; Evans, D. M.; Trim, J.; Juliano, M. A.; Scarisbrick, I. A.; Blaber, M.
22 Activation profiles of human kallikrein-related peptidases by proteases of the thrombostasis
23 axis. *Protein Sci* **2008**, 17, 1998-2007.

26
27 22. Shaw, M. A.; Gao, Z.; McElhinney, K. E.; Thornton, S.; Flick, M. J.; Lane, A.; Degen, J. L.;
28 Ryu, J. K.; Akassoglou, K.; Mullins, E. S. Plasminogen Deficiency Delays the Onset and Protects
29 from Demyelination and Paralysis in Autoimmune Neuroinflammatory Disease. *J Neurosci*
30 **2017**, 37, 3776-3788.

33
34 23. Balashov, K.; Dhib-Jalbut, S.; Rybinnik, I. Fibrinolysis induced clinical improvement in a
35 patient with multiple sclerosis exacerbation. *Mult Scler Relat Disord* **2020**, 43, 102225.

37
38 24. Masurier, N.; Arama, D. P.; El Amri, C.; Lisowski, V. Inhibitors of kallikrein-related
39 peptidases: An overview. *Med Res Rev* **2018**, 38, 655-683.

42
43 25. Prassas, I.; Eissa, A.; Poda, G.; Diamandis, E. P. Unleashing the therapeutic potential of
44 human kallikrein-related serine proteases. *Nat Rev Drug Discov* **2015**, 14, 183-202.

47
48 26. Masurier, N.; Soualmia, F.; Sanchez, P.; Lefort, V.; Roué, M.; Maillard, L.; Subra, G.;
49 Percot, A.; El Amri, C. Synthesis of Peptide–Adenine Conjugates as a New Tool for Monitoring
50 Protease Activity. *Eur. J. Org. Chem* **2019**, 2019, 176-183.
51
52
53
54
55
56
57
58
59
60

- 1
2
3 27. Loessner, D.; Goettig, P.; Preis, S.; Felber, J.; Bronger, H.; Clements, J. A.; Dorn, J.;
4
5 Magdolen, V. Kallikrein-related peptidases represent attractive therapeutic targets for ovarian
6
7 cancer. *Expert Opin Ther Targets* **2018**, *22*, 745-763.
8
9
10 28. Goettig, P.; Magdolen, V.; Brandstetter, H. Natural and synthetic inhibitors of
11
12 kallikrein-related peptidases (KLKs). *Biochimie* **2010**, *92*, 1546-1567.
13
14
15 29. Sananes, A.; Cohen, I.; Shahar, A.; Hockla, A.; De Vita, E.; Miller, A. K.; Radisky, E. S.;
16
17 Papo, N. A potent, proteolysis-resistant inhibitor of kallikrein-related peptidase 6 (KLK6) for
18
19 cancer therapy, developed by combinatorial engineering. *J Biol Chem* **2018**, *293*, 12663-
20
21 12680.
22
23
24 30. De Vita, E.; Schuler, P.; Lovell, S.; Lohbeck, J.; Kullmann, S.; Rabinovich, E.; Sananes, A.;
25
26 Hessling, B.; Hamon, V.; Papo, N.; Hess, J.; Tate, E. W.; Gunkel, N.; Miller, A. K. Depsipeptides
27
28 Featuring a Neutral P1 Are Potent Inhibitors of Kallikrein-Related Peptidase 6 with On-Target
29
30 Cellular Activity. *J Med Chem* **2018**, *61*, 8859-8874.
31
32
33 31. Soualmia, F.; Bosc, E.; Aït Amiri, S.; Stratmann, D.; Magdolen, V.; Darmoul, D.; Reboud-
34
35 Ravaux, M.; El Amri, C. Insights into the activity control of the kallikrein-related peptidase 6:
36
37 small-molecule modulators and allostereism. *Biol Chem.* **2018**, *399*, 1073-1078.
38
39
40 32. De Vita, E.; Smits, N.; van den Hurk, H.; Beck, E. M.; Hewitt, J.; Baillie, G.; Russell, E.;
41
42 Pannifer, A.; Hamon, V.; Morrison, A.; McElroy, S. P.; Jones, P.; Ignatenko, N. A.; Gunkel, N.;
43
44 Miller, A. K. Synthesis and Structure-Activity Relationships of N-(4-Benzamidino)-
45
46 Oxazolidinones: Potent and Selective Inhibitors of Kallikrein-Related Peptidase 6.
47
48 *ChemMedChem* **2020**, *15*, 79-95.
49
50
51 33. Liang, G.; Chen, X.; Aldous, S.; Pu, S. F.; Mehdi, S.; Powers, E.; Xia, T.; Wang, R. Human
52
53 kallikrein 6 inhibitors with a para-amidobenzylanmine P1 group identified through virtual
54
55 screening. *Bioorg Med Chem Lett* **2012**, *22*, 2450-2455.
56
57
58
59
60

- 1
2
3 34. Skaper, S. D. Oligodendrocyte precursor cells as a therapeutic target for demyelinating
4 diseases. *Prog Brain Res* **2019**, 245, 119-144.
5
6
7
8 35. Voet, S.; Prinz, M.; van Loo, G. Microglia in Central Nervous System Inflammation and
9 Multiple Sclerosis Pathology. *Trends Mol Med* **2019**, 25, 112-123.
10
11
12 36. Tamashiro, T. T.; Dalgard, C. L.; Byrnes, K. R. Primary microglia isolation from mixed
13 glial cell cultures of neonatal rat brain tissue. *J Vis Exp* **2012**, 15, e3814.
14
15
16
17 37. Bowes, J.; Brown, A. J.; Hamon, J.; Jarolimek, W.; Sridhar, A.; Waldron, G.; Whitebread,
18 S. Reducing safety-related drug attrition: the use of in vitro pharmacological profiling. *Nat Rev*
19 *Drug Discov* **2012**, 11, 909-922.
20
21
22
23 38. Strauss, K. I. Antiinflammatory and neuroprotective actions of COX2 inhibitors in the
24 injured brain. *Brain Behav Immun* **2008**, 22, 285-98.
25
26
27
28 39. Katayama, K.; Arai, Y.; Murata, K.; Saito, S.; Nagata, T.; Takashima, K.; Yoshida, A.;
29 Masumura, M.; Koda, S.; Okada, H.; Muto, T. Discovery and structure-activity relationships of
30 spiroindolines as novel inducers of oligodendrocyte progenitor cell differentiation. *Bioorg*
31 *Med Chem* **2020**, 28, 115348.
32
33
34
35 40. Zaldivar-Diez, J.; Li, L.; Garcia, A. M.; Zhao, W. N.; Medina-Menendez, C.; Haggarty, S.
36 J.; Gil, C.; Morales, A. V.; Martinez, A. Benzothiazole-Based LRRK2 Inhibitors as Wnt Enhancers
37 and Promoters of Oligodendrocytic Fate. *J Med Chem* **2020**, 63, 2638-2655.
38
39
40
41 41. Su, W.; Matsumoto, S.; Banine, F.; Srivastava, T.; Dean, J.; Foster, S.; Pham, P.;
42 Hammond, B.; Peters, A.; Girish, K. S.; Rangappa, K. S.; Basappa, J. J.; Hennebold, J. D.; Murphy,
43 M. J.; Bennett-Toomey, J.; Back, S. A.; Sherman, L. S. A modified flavonoid accelerates
44 oligodendrocyte maturation and functional remyelination. *Glia* **2020**, 68, 263-279.
45
46
47
48 42. Darensbourg, D. J.; Chung, W. C.; Arp, C. J.; Tsai, F. T.; Kyran, S. J. Copolymerization and
49 Cycloaddition Products Derived from Coupling Reactions of 1,2-Epoxy-4-cyclohexene and
50
51
52
53
54
55
56
57
58
59
60

1
2
3 Carbon Dioxide. Postpolymerization Functionalization via Thiol–Ene Click Reactions.
4
5 *Macromolecules* **2014**, 47, 7347–7353.
6

7
8 43. Tanaka, K. I.; Yoshifuji, S.; Nitta, Y. A New Method for the Synthesis of Amides from
9
10 Amines : Ruthenium Tetroxide Oxidation of N-Protected Alkylamines. *Chemical &*
11
12 *pharmaceutical bulletin* **1988**, 36, 3125-3129.
13

14
15 44. Gallo-Rodriguez, C.; Ji, X. D.; Melman, N.; Siegman, B. D.; Sanders, L. H.; Orlina, J.;
16
17 Fischer, B.; Pu, Q.; Olah, M. E.; van Galen, P. J.; Stiles, G. L.; Jacobson, K. A. Structure-activity
18
19 relationships of N6-benzyladenosine-5'-uronamides as A3-selective adenosine agonists. *J Med*
20
21 *Chem* **1994**, 37, 636-646.
22
23

24
25 45. Liang, G.; Chen, X.; Aldous, S.; Pu, S. F.; Mehdi, S.; Powers, E.; Giovanni, A.; Kongsamut,
26
27 S.; Xia, T.; Zhang, Y.; Wang, R.; Gao, Z.; Merriman, G.; McLean, L. R.; Morize, I. Virtual Screening
28
29 and X-ray Crystallography for Human Kallikrein 6 Inhibitors with an Amidinothiophene P1
30
31 Group. *ACS Med Chem Lett* **2012**, 3, 159-164.
32
33

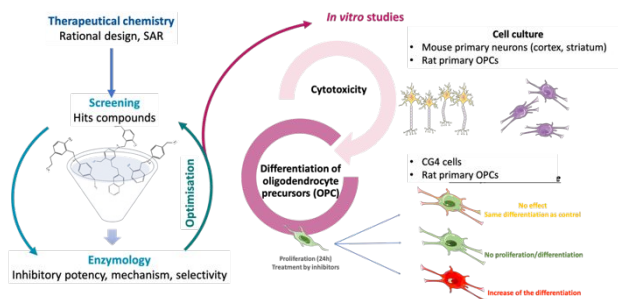
34
35 46. Olsson, M.; Søndergaard, C. R.; Rostkowski, M.; Jensen, J. H. PROPKA3: Consistent
36
37 Treatment of Internal and Surface Residues in Empirical pKa Predictions. *Journal of Chemical*
38
39 *Theory and Computation* **2011**, 7, 525-537.
40
41

42
43 47. Morris, G. M.; Huey, R.; Lindstrom, W.; Sanner, M. F.; Belew, R. K.; Goodsell, D. S.;
44
45 Olson, A. J. AutoDock4 and AutoDockTools4: Automated docking with selective receptor
46
47 flexibility. *J Comput Chem* **2009**, 30, 2785-2791.
48

49
50 48. Trott, O.; Olson, A. J. AutoDock Vina: improving the speed and accuracy of docking with
51
52 a new scoring function, efficient optimization and multithreading. *J Comput Chem* **2010**, 31,
53
54 455-461.
55
56
57
58
59
60

- 1
2
3 49. Kadukova, M.; Grudin, S. Convex-PL: a novel knowledge-based potential for protein-
4
5 ligand interactions deduced from structural databases using convex optimization. *J Comput*
6
7 *Aided Mol Des* **2017**, 31, 943-958.
8
9
10 50. Wegener, A.; Deboux, C.; Bachelin, C.; Frah, M.; Kerninon, C.; Seilhean, D.; Weider, M.;
11
12 Wegner, M.; Nait-Oumesmar, B. Gain of Olig2 function in oligodendrocyte progenitors
13
14 promotes remyelination *Brain* **2015**, 138, 120-135.
15
16
17 51. de Vellis, J.; Cole, R. Preparation of mixed glial cultures from postnatal rat brain.
18
19 *Methods Mol Biol* **2012**, 814, 49-59
20
21
22 52. Louis, J. C.; Magal, E.; Muir, D.; Manthorpe, M.; Varon, S. CG-4, a new bipotential glial
23
24 cell line from rat brain, is capable of differentiating in vitro into either mature
25
26 oligodendrocytes or type-2 astrocytes. *J Neurosci Res* **1992**, 31, 193-204.
27
28
29 53. Huang, J. K.; Jarjour, A. A.; Nait Oumesmar, B.; Kerninon, C.; Williams, A.; Krezel, W.;
30
31 Kagechika, H.; Bauer, J.; Zhao, C.; Baron-Van Evercooren, A.; Chambon, P.; Ffrench-Constant,
32
33 C.; Franklin, R. J. M. Retinoid X receptor gamma signaling accelerates CNS remyelination. *Nat*
34
35 *Neurosci* **2011**, 14, 45-53.
36
37
38
39
40
41
42
43
44
45
46
47
48
49
50
51
52
53
54
55
56
57
58
59
60

Table of content graphic



1
2
3
4
5
6
7
8
9
10
11
12
13
14
15
16
17
18
19
20
21
22
23
24
25
26
27
28
29
30
31
32
33
34
35
36
37
38
39
40
41
42
43
44
45
46
47
48
49
50
51
52
53
54
55
56
57
58
59
60